The conserved ATPase PCH-2 controls the number and distribution of crossovers by antagonizing crossover formation in *C. elegans*

Bhumil Patel, Maryke Grobler, Alberto Herrera, Elias Logari, Valery Ortiz, and Needhi Bhalla[1]

Department of Molecular, Cell and Developmental Biology, University of California, Santa Cruz, Santa Cruz, CA 95064

[1] corresponding author: nbhalla@ucsc.edu
Department of Molecular, Cell and Developmental Biology
225 Sinsheimer Labs
University of California, Santa Cruz
Santa Cruz, CA 95064
phone: (831) 459-1319
fax: (831) 459-3139

Abstract

Meiotic crossover recombination is essential for both accurate chromosome segregation and the generation of new haplotypes for natural selection to act upon. While the conserved role of the ATPase, PCH-2, during meiotic prophase has been enigmatic, a universal phenotype that is observed when *pch-2* or its orthologs are mutated is a change in the number and distribution of meiotic crossovers. Here, we show that PCH-2 controls the number and distribution of crossovers by antagonizing crossover formation. This antagonism produces different effects at different stages of meiotic prophase: early in meiotic prophase, PCH-2 prevents double strand breaks from becoming crossovers, limiting crossovers at sites of initial DSB formation and homolog interactions. Later in meiotic prophase, PCH-2 winnows the number of crossover-eligible intermediates, contributing to the reinforcement of crossover-eligible intermediates, designation of crossovers and ultimately, crossover assurance. We also demonstrate that PCH-2 accomplishes this regulation through the meiotic HORMAD, HIM-3. Our data strongly support a model in which PCH-2's conserved role is to remodel meiotic HORMADs throughout meiotic prophase to destabilize crossover-eligible precursors, coordinate meiotic recombination with synapsis, and contribute to the progressive implementation of meiotic recombination, guaranteeing crossover control.

Introduction

Meiosis is a specialized type of cell division that reduces chromosome number by half, resulting in the production of four genetically diverse haploid gametes, so that fertilization during sexual reproduction restores diploidy. This process occurs in two stages: meiosis I, in which homologous chromosomes are partitioned, and meiosis II, in which sister chromatid are segregated. The regulation of meiosis is crucial for ensuring that both genetic recombination and chromosome segregation occur accurately. During prophase I, homologous chromosomes pair and this pairing is stabilized through a process called synapsis, in which a protein structure called the synaptonemal complex (SC) holds homologs together. This close association between homologs during synapsis facilitates crossover formation, the process in which double strand breaks (DSBs) are deliberately introduced into the genome, repaired by meiosis-specific mechanisms that exchange DNA between homologous chromosomes and generate the chiasmata, or linkage, that promotes accurate meiotic chromosome segregation. Therefore, disruptions in pairing, synapsis, or recombination prevent the formation of chiasmata and can lead to meiotic errors such as nondisjunction, resulting in aneuploid gametes. Errors in human meiosis are associated with birth defects, such as Down and Turner syndromes, infertility and miscarriages, underscoring the importance of understanding meiosis to human health (Hassold & Hunt, 2001).

In addition to the fundamental role that recombination plays in ensuring accurate chromosome segregation, crossover recombination accomplishes another important function: it generates new haplotypes for natural selection to act upon to drive evolution. Thus, to assure a random assortment of alleles on a population level, the distribution of crossovers may be as tightly regulated as their number. The significance of controlling both crossover number and distribution is clearly illustrated by the existence of mechanisms such as crossover assurance, in which every pair of homologous chromosomes gets at least one crossover; crossover homeostasis, in which the number of crossovers remains relatively invariant even if the number of recombination precursors change; and crossover

interference, in which the presence of a crossover inhibits the formation of a crossover nearby (Gray & Cohen, 2016). DSBs typically vastly outnumber crossovers in most organisms and are introduced gradually throughout early prophase. Therefore, to accomplish this precise level of control, meiotic crossover recombination and the decision about which DSBs become crossover-eligible intermediates, and eventually crossovers, is implemented progressively throughout meiotic prophase (Cole et al., 2012; Joshi et al., 2015; Morgan et al., 2021; Yokoo et al., 2012).

PCH-2, also known as TRIP13 in mammals, is an evolutionarily ancient AAA-ATPase that plays a significant role in regulating meiosis across different organisms, including *M. musculus* (mice), *S. cerevisiae* (budding yeast), *D. melanogaster* (fruit flies), and *C. elegans* (worms) (Bhalla, 2023). PCH-2 and its orthologs structurally remodel a family of proteins with HORMA domains (HORMADs) to control their function (Gu et al., 2022). HORMADs participate in a variety of signaling events and can exist in at least three structurally distinct conformations: a “closed” conformation, which they adopt when they bind a short peptide sequence in their own protein sequence or another protein (also called a closure motif) and their C-terminus wraps around this motif to stabilize the interaction; an “open” conformation when unbound, in which their C-terminus is discretely tucked against the HORMA domain; and an “extended” conformation, which is an intermediate between the two (Gu et al., 2022). PCH-2 and its orthologs convert the closed version of HORMADs to the open or extended versions, playing an important role in recycling HORMADs during signaling. During meiosis, closed versions of meiotic HORMADs assemble on chromosomes to form meiotic chromosome axes, which are essential for pairing, synapsis and recombination between homologous chromosomes (Kim et al., 2014). The remodeling of meiotic HORMADs by PCH-2 to an “open” or “extended” conformation is thought to reduce the levels of HORMADs on chromosomes (Börner et al., 2008; Cuacos et al., 2021; Lambing et al., 2015; Wojtasz et al., 2009) and/or increase their dynamic association and dissociation (Russo et al., 2023), modulating and coordinating homolog pairing, synapsis and recombination during prophase.

The conserved role of the PCH-2/HORMAD module in meiosis has been difficult to characterize, in part, we have argued, because of the evolutionary innovation that is an inherent aspect of sexual reproduction (Bhalla, 2023). Moreover, in some systems, such as budding yeast and plants (Herruzo et al., 2021; Yang et al., 2020), PCH-2 orthologs not only remodel meiotic HORMADs on meiotic chromosomes but also perform this function in the cytoplasm to make meiotic HORMADs available for their role(s) in meiotic nuclei. This dual role can complicate functional analyses, particularly in *pch-2* null mutants. However, all meiotic systems exhibit defects in the number and distribution of crossovers when PCH-2 function is abrogated by mutation (Deshong et al., 2014; Joshi et al., 2009; Joyce & McKim, 2009; Lambing et al., 2015; Roig et al., 2010; Zanders & Alani, 2009). Unfortunately, the lack of a clear pattern when analyzing these defects in recombination in *pch-2* mutants has contributed to an inability to develop a unified, integrated model of PCH-2 function in the field.

In *C. elegans*, meiotic HORMADs localize to meiotic chromosomes independently of PCH-2 (Deshong et al., 2014). Here, we exploit this system to show that PCH-2 is required to control the number and distribution of crossovers by antagonizing the formation of crossovers. This antagonism produces different consequences depending on the stage of meiotic prophase. In early meiotic prophase, PCH-2 inhibits DSBs from becoming crossovers, ensuring that they are more widely distributed than sites of initial DSB formation and/or homolog interactions. Later in meiotic prophase, PCH-2 is responsible for winnowing the numbers of crossover-eligible intermediates on synapsed chromosomes, contributing to the reinforcement of crossover-eligible intermediates, designation of crossovers and ultimately, crossover assurance. Genetic analysis demonstrates that PCH-2's regulation of crossover-eligible intermediates is through one of three essential meiotic HORMADs, HIM-3. Finally, we link PCH-2's effect on early DSBs in early meiotic prophase to cell cycle stage, demonstrating that both limit early DSBs from becoming crossovers. We propose that PCH-2's remodeling of HIM-3 on meiotic chromosomes destabilizes crossover-eligible intermediates throughout meiotic prophase, contributing to the progressive implementation of meiotic recombination to control the number and distribution of crossovers and accomplish crossover control.

Results

PCH-2 controls the number and distribution of crossovers in similar patterns on multiple chromosomes

We had previously shown that loss of PCH-2 reduced the frequency of double crossovers and genetic length of both an autosome (chromosome III) and the X chromosome, albeit not uniformly among genetic intervals (Deshong et al., 2014). To determine whether a more obvious pattern could be observed, we expanded our analysis by monitoring recombination genetically in both wildtype and *pch-2* mutant animals using five single nucleotide polymorphisms (SNPs) that spanned 95% of Chromosomes, I, III, IV and the X chromosome (Figure 1). We excluded Chromosome II from our analysis because of the potential difficulty combining Hawaiian SNPs with the *pch-2* mutation, which is linked to Chromosome II, and Chromosome V because of our use of the *bcIs39* transgene to identify cross progeny, which may disrupt recombination on that chromosome.

In wildtype animals, we observed multiple double crossovers, ranging from 1-13 depending on the chromosome. In a majority of these double crossovers (69%), one crossover was at the end of the chromosome where pairing and synapsis initiate, also called the Pairing Center (PC) (MacQueen et al., 2005), suggesting some relationship between where chromosomes might make initial contacts and the likelihood of double crossovers. On all chromosomes analyzed, we observed no double crossovers in *pch-2* mutants and this difference was statistically significant for Chromosomes I, III and X. Moreover, there was a striking shift of crossovers to the PC end of all four chromosomes tested. This shift in the distribution of crossovers to the PC ends of chromosomes was generally accompanied by a reduction in crossovers in the center of chromosomes. In *C. elegans*, the center of chromosomes are where double strand breaks are less numerous (Nadarajan et al., 2021; Yu et al., 2016) and where genes are more abundant. In the case of the X chromosome and chromosome III, recombination at the non-PC end was also reduced and appeared to more closely resemble the physical map at this

end of these chromosomes. Thus, PCH-2 ensures a wider distribution of crossovers across chromosomes, away from regions that are more likely to undergo early homolog interactions (PC ends) and with more double strand breaks (both the PC and non-PC ends of chromosomes), and towards the center of chromosomes, where double strand breaks are less abundant.

PCH-2 prevents exogenous DSBs early in meiotic prophase from becoming crossovers

We previously showed that PCH-2 promotes crossover formation and crossover assurance through its regulation of the meiotic HORMAD, HIM-3, in *C. elegans* (Russo et al., 2023). Moreover, this promoting role seems linked to its localization to the synaptonemal complex (Patel et al., 2023). However, the observed shift in the distribution of crossovers in *pch-2* mutants suggests that PCH-2 may also play a role in inhibiting crossovers and that this role may be occurring in early meiotic prophase, when chromosomes are undergoing initial homolog interactions. Previous data from our lab had suggested this possibility, but experimental caveats limited our ability to properly interpret these experiments (Deshong et al., 2014).

To explicitly test this possibility, we took advantage of both the spatiotemporal organization of meiotic nuclei in the *C. elegans* germline, and the observation that nuclei travel in an assembly line process at a stereotypical pace to late pachytene (Jaramillo-Lambert et al., 2007), where we can cytologically assess crossover formation by staining for the essential crossover factor, COSA-1 (Yokoo et al., 2012). We performed irradiation experiments to introduce exogenous DSBs at different timepoints during meiotic prophase and analyzed PCH-2's role in crossover formation (Figure 2A).

In this experiment, we tested the effects of ionizing radiation at two distinct time points: 8 hours after irradiation, when we can monitor crossover formation in meiotic nuclei that received exogenous DSBs in mid-pachytene, and 24 hours after irradiation, when we monitor crossover formation in meiotic

nuclei that received exogenous DSBs in leptotene/zygotene, also known as the transition zone in *C. elegans*. In order to detect crossovers, control and *pch-2* mutants germlines were stained for GFP::COSA-1, which allowed us to visualize crossovers, and DAPI, which allowed us to visualize DNA. At 8 hours after irradiation, we observed a significant increase in nuclei containing less than 6 COSA-1 nuclei in *pch-2* mutants (26%), when compared to control (9%) germlines (Figure 2B, 2C). We did not observe a significant number of nuclei with greater than 6 COSA-1 foci in either backgrounds. This observation is consistent with our and others' previous findings: exogenous DSBs in mid-pachytene do not affect the number of crossovers in wildtype animals (Yokoo et al., 2012) and loss of PCH-2 leads to a decrease in crossover formation (Deshong et al., 2014).

Next, we examined crossover formation 24 hours post-irradiation (Figure 2D, 2E). For this time point, we also saw a significant increase in nuclei containing less than 6 COSA-1 foci (control: 13%, *pch-2*: 26%), similar to the 8 hour time point. However, in contrast to the 8 hour time point, we also observed a significant increase in nuclei with more than 6 COSA-1 foci in *pch-2* mutants (wildtype: 2%, *pch-2*: 13%), indicating that loss of PCH-2 leads to increased crossover formation when nuclei in the transition zone get more DSBs. In other words, PCH-2 inhibits exogenous DSBs in early meiotic prophase from becoming crossovers, consistent with our analysis of recombination on multiple chromosomes.

PCH-2 prevents SPO-11-induced DSBs from becoming crossovers in early meiotic prophase

Our previous experiment indicated that PCH-2 is preventing exogenous DSBs in early meiotic prophase from becoming crossovers (Figure 2). To test whether this was also the case for programmed meiotic DSB formation, we used the auxin-inducible degradation (AID) system to remove the enzyme that is responsible for programmed meiotic DSBs, SPO-11 (*spo-11::AID::3XFLAG*) (Dernburg et al., 1998; Keeney et al., 1997). Since meiotic nuclei travel through the germline at about one cell per row per hour (Jaramillo-Lambert et al., 2007), we took advantage of this precise

spatiotemporal resolution to test five different timepoints to determine if acute depletion of SPO-11 leads to any changes in crossover formation between control animals and *pch-2* mutants (Figure 3A). We assayed crossover formation by analyzing both the number of GFP::COSA-1 foci in late pachytene and the presence of bivalents in diakinesis, which indicates the successful formation of chiasmata between homologous chromosomes. Meiotic nuclei travel from late pachytene to diakinesis in approximately 12 hours (Deshong et al., 2014).

When we treated both control and *pch-2* mutant worms for 36 hours with auxin, we observed a complete loss of GFP::COSA-1 foci (Figure 3C). When these animals were treated with auxin for 48 hours, to allow nuclei without SPO-11 an additional 12 hours to reach diakinesis, we observed 12 DAPI stained bodies, or univalents, which are the 6 homolog pairs that have not formed chiasmata (Figure 3E). Thus, we can reliably remove SPO-11 from meiotic nuclei throughout the germline and prevent crossover formation.

Having established that we can reliably remove SPO-11 with the AID system, we performed the same experiment at additional timepoints that remove SPO-11 at different stages of early meiotic prophase, monitoring crossover formation both at late pachytene and 12 hours later in diakinesis: 24 hours to monitor GFP::COSA-1 foci and 36 hours to monitor bivalent formation; 22 (GFP::COSA-1 foci) and 34 (bivalent formation) hours; 20 (GFP::COSA-1 foci) and 32 hours (bivalent formation); and 18 (GFP::COSA-1 foci) and 30 hours (bivalent formation). We also performed a control experiment, treating worms with ethanol for the 24 and 36 hour timepoints to ensure that this tagged version of SPO-11 was fully functional for crossover formation (Figure 3C, 3D).

At the 24 hour time point, when meiotic nuclei in the transition zone do not receive SPO-11-induced DSBs, we observe a range of GFP::COSA-1 foci in late pachytene in both control animals and *pch-2* mutants with a majority of nuclei having 0 or 1 focus (control and *pch-2* averages: 1.8 GFP::COSA-1 foci), indicating a loss of crossover formation, albeit with some heterogeneity. This was confirmed

when we monitored bivalent formation at the 36 hour timepoint in both strains. This heterogeneity likely reflects that it takes 1-4 hours to significantly affect DSB formation through acute degradation of SPO-11 at this stage of meiosis in *C. elegans* (Hicks et al., 2022). In addition, there was no statistically significant difference in the number of GFP::COSA-1 foci between control animals and *pch-2* mutants. However, we did observe a slight, statistically significant difference in the number of DAPI stained bodies between control animals (average number of DAPI stained bodies: 10.6) and *pch-2* mutants (average number of DAPI stained bodies: 9.6), suggesting that even at this very early time point, we can detect a role for PCH-2 in preventing early SPO-11-induced DSBs from becoming crossovers (Figure 3D, 3E).

We continued to monitor GFP::COSA-1 and bivalent formation at successive timepoints. At the 22 hours and 34 hour timepoints, where SPO-11 depletion begins later in the transition zone, we saw an increase in the number of GFP::COSA-1 foci and a reduction in the number of DAPI stained bodies, suggesting that more DSBs are becoming crossovers. This trend continued at the 20 hour and 32 hour timepoints, eventually reaching wildtype numbers for GFP::COSA-1 and DAPI stained bodies by the 18 hour and 30 hour timepoints, respectively.

At the 22 hour and 36 hour timepoints, we did not detect any statistically significant difference in the number of GFP::COSA-1 foci or DAPI stained bodies between control animals and *pch-2* mutants, even when we analyzed the number of nuclei that had greater than 6 GFP::COSA-1 foci. In contrast, while the number of GFP::COSA-1 foci was not statistically significantly different between control animals and *pch-2* mutants at the 20 hour time point, the number of nuclei with greater than 6 GFP::COSA-1 foci was significantly higher in *pch-2* mutants (control: 3%, *pch-2*: 10%, p value = 0.009, Fischer's Exact Test), similar to our analysis of GFP::COSA-1 24 hours after irradiation. Even more strikingly, the number of DAPI stained bodies was significantly lower in *pch-2* animals than control animals at the corresponding 32 hour timepoint, indicating that more homolog pairs had successfully formed chiasmata in *pch-2* mutants. The inconsistency between the average number of

GFP::COSA-1 foci and DAPI stained bodies at this time point can be explained by our ability to more reliably detect *pch-2*'s loss of crossover assurance when quantifying GFP::COSA-1 foci than when analyzing bivalent formation (Deshong et al., 2014; Russo et al., 2023). No difference in GFP::COSA-1 foci or bivalent formation was observed at the 18 hour and 30 hours timepoints, respectively. These data indicate that during a narrow time frame of early meiotic prophase, likely during leptotene/zygotene given the delay in limiting DSB formation with auxin-induced degradation of SPO-11, PCH-2 prevents SPO-11-induced DSBs from becoming crossovers and chiasmata.

PCH-2 is required for timely loading and removal of MSH-5 on meiotic chromosomes through its regulation of HIM-3

After DSB formation, a subset of DSBs are repaired through a pro-crossover pathway and eventually winnowed to a stereotypical number of crossovers. In *C. elegans*, this can be visualized by the loading of the pro-crossover factor MSH-5, a component of the meiosis-specific MutS γ complex that stabilizes crossover-specific DNA repair intermediates called joint molecules (Janisiw et al., 2018; Kelly et al., 2000; Snowden et al., 2004). GFP::MSH-5 begins to form a few foci in the transition zone, becoming more numerous in early pachytene before decreasing in number in mid pachytene to ultimately colocalize with COSA-1 marked sites in late pachytene (Janisiw et al., 2018; Woglar & Villeneuve, 2018; see control in Figure 4A, 4B). The mechanism through which MSH-5 functions with the SC and other meiosis factors to ultimately form crossovers has not been established but may involve phosphorylation by cyclin-dependent kinases (Haversat et al., 2022; Zhang et al., 2021).

Given that we have shown that PCH-2 prevents early DSBs from becoming crossovers (Figures 2 and 3), we tested whether we could cytologically detect this inhibition at the level of MSH-5 behavior in control animals and *pch-2* mutants. We generated wildtype and *pch-2* mutants with GFP::MSH-5 and quantified the average number of GFP::MSH-5 foci per row of nuclei from the transition zone to late

pachytene (Figure 4A, 4B). We observed a statistically significant increase in the average number of GFP::MSH-5 foci per row in the transition zone in *pch-2* mutants (Figure 4A, 4B, p value < 0.0001, Student's t-test), indicating that PCH-2 typically limits MSH-5 loading at this early stage of meiotic prophase. The average number of GFP::MSH-5 foci per row were similar in number in early pachytene in both backgrounds. However, we also observed a substantial increase in the average number of GFP::MSH-5 foci per row in *pch-2* mutants in the mid and late pachytene regions (Figure 4A, 4B), indicating that PCH-2 also promotes the turnover or maturation of GFP::MSH-5 foci at these later stages of meiotic prophase. Thus, PCH-2 prevents the loading of the crossover-promoting factor, MSH-5, during early meiotic prophase, consistent with both our genetic analysis of recombination (Figure 1) and its role in preventing early DSBs from becoming crossovers (Figures 2 and 3). However, PCH-2 also appears to limit the number of crossover-eligible intermediates in mid and late pachytene, an unexpected observation given that the most severe recombination defect in *pch-2* mutants is the loss of crossover assurance (Deshong et al., 2014).

We previously showed that PCH-2 genetically interacts with meiotic HORMADs to effectively control different aspects of meiosis: PCH-2 regulates pairing and synapsis through its regulation of HTP-3 and crossover recombination through its regulation of HIM-3 (Russo et al., 2023). To determine which meiotic HORMAD PCH-2 might be regulating to affect GFP::MSH-5's loading and removal on meiotic chromosomes, we constructed *gfp::msh-5;htp-3*^{H96Y}*, gfp::msh-5;pch-2;htp-3*^{H96Y}*, gfp::msh-5;him-3*^{R93Y} and *gfp::msh-5;pch-2;him-3*^{R93Y} mutants and quantified GFP::MSH-5 foci throughout the germline. Both *htp-3*^{H96Y} and *him-3*^{R93Y} mutants showed a drastic increase in the average number of GFP::MSH-5 per row of nuclei throughout the germline (Figures 4C and 4D, Supplemental Figure 1). For example, compared to control germlines that peaked at approximately an average of 20 MSH-5 foci per row in early pachytene and then decreased in mid-pachytene, *him-3*^{R93Y} germlines had closer to an average of 30 GFP::MSH-5 foci per row in early pachytene. Moreover, the average number of GFP::MSH-5 foci per row increased further in mid and late pachytene, achieving peaks closer to an average of 35 foci (Figure 4D). These very high numbers of GFP::MSH-5 were striking but do not

produce an increased number of crossovers in *htp-3*^{H96Y} or *him-3*^{R93Y} single mutants (Russo et al., 2023), raising the possibility that not all of them reflect functional, crossover-specific intermediates, similar to what has been observed in the absence of synapsis (Woglar & Villeneuve, 2018). These data also suggest that these mutations, which disrupt the ability of meiotic HORMADs to adopt the "closed" conformation (Russo et al., 2023), affect the behavior of GFP::MSH-5 on meiotic chromosomes.

Quantification of GFP::MSH-5 foci in *pch-2;htp-3*^{H93Y} double mutants was similar to *htp-3*^{H93Y} single mutants, suggesting that PCH-2's effect on the behavior of GFP::MSH-5 foci was not through its regulation of HTP-3 (Supplemental Figure 1). In stark contrast to *pch-2;htp-3*^{H93Y} double mutants, the *pch-2*;*him-3*^{R93Y} double mutant showed a dramatic decrease in the overall average of MSH-5 foci per row throughout the germline (Figure 4C, 4D). These averages fell between the averages in control and *pch-2* mutant animals, particularly in the transition zone and late pachytene (Figure 4D), consistent with our previous report that this double mutant has fewer defects in crossover formation than either single mutant (Russo et al., 2023). These data indicate that PCH-2's effect on promoting the removal of GFP::MSH-5 in both the transition zone and mid to late pachytene is through its regulation of HIM-3.

pch-2 single mutants exhibit a loss of crossover assurance (Deshong et al., 2014). However, our quantification of GFP::MSH-5 in *pch-2* single mutants in mid to late pachytene showed an increased number of crossover-eligible intermediates (Figure 4A, 4B), suggesting a complex relationship between having too many crossover-eligible intermediates and crossover assurance in *C. elegans*. To address this inconsistency, we generated strains with both OLLAS::COSA-1 (Janisiw et al., 2018) and GFP::MSH-5 in wildtype animals and *pch-2* mutants. Consistent with our and others' previous findings, we observe a gradual reduction in the average number of GFP::MSH-5 foci per row of nuclei in control animals as these nuclei approach the end of pachytene, ultimately converging with the average

number of OLLAS::COSA-1 foci per row (Figure 4E, 4F) (Janisiw et al., 2018; Woglar & Villeneuve, 2018). In addition, we consistently observed co-localization of GFP::MSH-5 and OLLAS::COSA-1 foci in control animals, with a few MSH-5 foci persisting without COSA-1 (Figure 4E, 4F).

By contrast, we detected higher average numbers of GFP::MSH-5 foci per row across all late pachytene nuclei in *pch-2* mutants and this average never converged upon the average number of OLLAS-1::COSA-1 foci per row (Figure 4E, 4F). To test whether there was a correlation between the number of GFP::MSH-5 foci and the loss of crossover assurance in *pch-2* mutants, we determined the average number of GFP::MSH-5 foci in meiotic nuclei with 6 OLLAS::COSA-1 foci and those with less than 6 OLLAS::COSA-1 foci in both control and *pch-2* mutant animals (Figure 4E, 4G, Supplemental Figure 2). Indeed, we observed that *pch-2* mutant nuclei with less than 6 OLLAS::COSA-1 foci had significantly higher numbers of GFP::MSH-5 foci, compared to both control and *pch-2* mutant nuclei with 6 OLLAS::COSA-1 foci (Figure 4E, 4G), suggesting that the inability to reduce the number of crossover-eligible intermediates in *pch-2* mutants, counterintuitively, contributes to the observed loss of crossover assurance.

PCH-2 is removed from the synaptonemal complex when crossovers are designated

We have previously shown that PCH-2 localization to the SC is extended when there are partial defects in synapsis or changes in karyotype, producing an increase in crossovers and a loss of crossover interference (Deshong et al. 2014; Patel et al., 2023). These data led us to hypothesize that PCH-2's presence on chromosomes promotes crossover formation. However, our quantification of GFP::MSH-5 indicates that PCH-2 is required to limit the number of crossover-eligible intermediates, in direct contrast to our proposed hypothesis (Figure 4). Therefore, we decided to revisit what role PCH-2 localization to the SC might play in regulating crossover formation. To this end, we localized PCH-2 in *dsb-2* mutants, in which DSB formation is substantially reduced and fewer crossovers are formed in *C. elegans* (Rosu et al., 2013). We performed this experiment because, in budding yeast,

similar mutants that reduce DSB formation rely on Pch2 to successfully complete meiosis (Joshi et al., 2009; Zanders & Alani, 2009).

Because the recombination defect in *dsb-2* mutants worsens with age (Rosu et al., 2013), we looked at PCH-2 localization in both young (24 hours post L4 larval stage) and older animals (48 hours post L4). We observed a unique and striking localization pattern in *dsb-2* mutants that we had not observed before. When stained for PCH-2 and GFP::COSA-1, nuclei retain PCH-2 onto chromosomes far into late pachytene, past the normal region when PCH-2 typically is removed from chromosomes (Figure 5A, 5B). However, unlike what we have observed in other mutants that have defects in synapsis or changes in karyotype, this retention of PCH-2 is not uniform among all late pachytene nuclei in *dsb-2* mutants. Instead, most nuclei lose PCH-2 localization in late pachytene while some retain it. We tested whether there was a relationship between the retention of PCH-2 and the number of GFP::COSA-1 foci and found that 96% of nuclei that lose PCH-2 have at least 1 GFP::COSA-1 focus (Figure 5A, 5B). In older animals (see 48 hours post-L4), this pattern was even more clear: 77% of nuclei without PCH-2 had 1 or more GFP::COSA-1 focus and 93% of meiotic nuclei without a GFP::COSA-1 focus retained PCH-2.

These data indicate that PCH-2's removal from the SC is in response to, coincident with or facilitates crossover designation. To distinguish between these possibilities, we analyzed GFP::COSA-1 foci in *dsb-2::AID* (Zhang et al., 2018) and *dsb-2::AID;pch-2* worms, reasoning that if PCH-2's removal is in response to or coincident with designation, we should not detect any differences in the number of GFP::COSA-1 foci in *dsb-2::AID* and *dsb-2::AID;pch-2* worms. We performed these experiments with the auxin-inducible degradation system because of variability in the *dsb-2* mutant background that affected reproducibility of our experiments.

Upon auxin treatment of *dsb-2::AID* worms, we observed a statistically significant (p value < 0.0001, Mann-Whitney U test) decrease in the number of GFP::COSA-1 foci, in comparison with ethanol-treated worms, verifying that we can reliably knock down DSB-2 with the AID system (Figure 5D). When we performed the same experiment in *dsb-2::AID;pch-2* worms, the average number of GFP::COSA-1 foci further decreased, indicating that fewer crossovers are designated when DSBs are reduced and PCH-2 is absent (Figure 5C, 5D). These data suggest that PCH-2's presence on the SC prevents crossover designation. Given the correlation between elevated GFP::MSH-5 foci and the loss of crossover assurance we observe in *pch-2* mutants, we propose that PCH-2 is retained on meiotic chromosomes to ensure that extra crossover-eligible intermediates are removed and crossover designation is delayed until crossover assurance can be guaranteed in *C. elegans*.

PCH-2 and high CHK-2 activity control the fate of early double strand breaks

In *C. elegans*, meiotic cell cycle entry and progression depends on the activity of CHK-2, the meiosis-specific ortholog of the DNA-damage kinase Chk2/CHEK2 (Baudrimont et al., 2022; Castellano-Pozo et al., 2020; Kim et al., 2015; MacQueen & Villeneuve, 2001; Zhang et al., 2023). Meiotic nuclei in leptotene/zygotene are characterized by high CHK-2 activity, which drops to intermediate activity in mid-pachytene (Kim et al., 2015; Zhang et al., 2023). In late pachytene, CHK-2 activity is inactivated by the recruitment of polo-like kinase, PLK-2, to the SC, which enables crossover designation (Zhang et al., 2023). Thus, CHK-2 activity also has consequences for the progression of meiotic recombination and DNA repair.

Given that early DSBs are prevented from becoming crossovers by PCH-2 in early meiotic prophase, we wanted to test if high CHK-2 activity in leptotene/zygotene also contributed to the fate of these early DSBs. To evaluate this possibility, we used *syp-1*^{T452A} mutants (Sato-Carlton et al., 2018). The SC component, SYP-1, is phosphorylated by CDK-1 on T452, producing a Polo box binding motif that recruits PLK-2 to the SC, contributing to the inactivation of CHK-2 when chromosomes are synapsed

(Brandt et al., 2020; Zhang et al., 2023). Therefore, in *syp-1*^{T452A} mutants, CHK-2 activity remains high throughout most of meiotic prophase in the *C. elegans* germline (Figure 6A).

We quantified the total number of GFP::COSA-1 foci in late pachytene nuclei in *syp-1*^{T452A} mutants and observed a significant decrease in the average number of GFP::COSA-1 foci when compared to control animals (Figures 6B and 6C), consistent with previous findings that *syp-1*^{T452A} mutants delay designation and have fewer crossovers (Zhang et al., 2023). These data are also consistent with the possibility that some DSBs fail to become crossovers when CHK-2 activity remains high. If this hypothesis is correct, we predict that the combination of high CHK-2 activity and loss of *pch-2* should produce more crossovers. We generated *pch-2;syp-1*^{T452A} double mutants to test this hypothesis. When we quantified GFP::COSA-1 in *pch-2;syp-1*^{T452A} double mutants, we detected a significant increase in the average number of GFP::COSA-1 foci compared to *syp-1*^{T452A} single mutants (Figure 6C), in strong support of our hypothesis.

To further verify that the *pch-2* mutation suppresses the crossover defect in *syp-1*^{T452A} mutants, we also monitored bivalent formation in diakinesis nuclei. *syp-1*^{T452A} single mutants exhibit an average of 7.12 DAPI staining bodies in diakinesis, higher than both control animals and *pch-2* single mutants (Figure 6D). By contrast, *pch-2;syp-1*^{T452A} mutants had an average of 6.05 DAPI staining bodies (Figure 6D, 6E), directly supporting our COSA-1 analysis and indicating that both PCH-2 function and high CHK-2 activity collaborate to control the fate of DSBs and prevent some of them from becoming crossovers in early meiotic prophase.

Discussion

We have shown that PCH-2 antagonizes crossover formation throughout meiotic prophase and that this regulation occurs through one of the three essential meiotic HORMADs in *C. elegans*, HIM-3

(Figure 4). We propose that PCH-2 remodels HIM-3 on meiotic chromosomes to destabilize crossover-eligible intermediates, thus limiting which DSBs will become crossovers (Figure 7). However, this antagonism has different consequences depending on when during meiotic prophase it occurs, underscoring the importance of temporal regulation of these events. During leptotene/zygotene, when CHK-2 activity is high (Kim et al., 2015; Zhang et al., 2023) and PCH-2 is present as foci on chromosomes (Deshong et al., 2014), PCH-2 prevents crossover formation at some sites of initial DSB formation and early homolog interactions (Figure 7B). In this way, PCH-2 promotes a wider distribution of crossovers across the genome (Figure 1). In pachytene, when CHK-2 activity has decreased (Kim et al., 2015; Zhang et al., 2023) and PCH-2 is localized to the SC (Deshong et al., 2014), PCH-2 winnows crossover-eligible intermediates, ensuring their reinforcement, designation and crossover assurance (Figure 7B). When there are defects in recombination, such as partial synapsis (Deshong et al., 2014), changes in karyotype (Patel et al., 2023) or too few DSBs (Figure 5), PCH-2 persists on the SC to prevent designation, guarantee crossover assurance and some degree of homeostasis, independent of an additional feedback mechanism that increases DSB formation (Patel et al., 2023). That persistence of PCH-2 also disrupts crossover interference in two of these situations (Deshong et al., 2014; Patel et al., 2023) strongly suggests that crossover interference is mechanistically linked to assurance and homeostasis.

him-3^{R93Y};pch-2 double mutants have stronger crossover assurance than either single mutant but less than wildtype animals (Russo et al., 2023), a phenotype which can now be explained by the behavior of GFP::MSH-5 foci in these double mutants (Figure 4C, 4D). We have shown that HIM-3^{R93Y} mutant protein can adopt the closed conformation and loads on meiotic chromosomes similar to wildtype HIM-3 (Russo et al. 2023). In vitro analysis shows that HIM-3^{R93Y} binds its closure motif with reduced affinity, likely affecting its ability to adopt the closed conformation in vivo (Figure 7A and Russo et al. 2023). The proposed role of PCH-2 in meiosis is to remodel meiotic HORMADs from the closed conformation to the extended one (Figure 7A), regulating their association with chromosomes (Bhalla, 2023). However, since meiotic HORMADs are not visibly depleted from chromosomes during meiotic

progression in *C. elegans* (Couteau et al., 2004; Couteau & Zetka, 2005; Goodyer et al., 2008; Martinez-Perez & Villeneuve, 2005), this genetic interaction supports a role for PCH-2 in temporarily reducing the occupancy of meiotic HORMADs on meiotic chromosomes, destabilizing interactions with partner proteins that modulate the progression and fidelity of meiotic recombination (Russo et al., 2023). Thus, PCH-2's remodeling of HIM-3 would disrupt protein-protein interactions that underlie crossover-eligible intermediates, destabilizing them and reducing their number on chromosomes, contributing to crossover control (Figure 7B). Since meiotic HORMADs are essential for meiotic chromosome axis structure and function, our data therefore support a role for the meiotic axis in crossover control, as suggested by previous reports (Chu et al., 2024; Girard et al., 2023; Lambing et al., 2020; Nabeshima et al., 2004). However, the disassembly of crossover-eligible intermediates would also release pro-crossover factors present at these sites to concentrate at other, more stable sites on the SC, contributing to reinforcement and designation during synapsis (Girard et al., 2023; Yokoo et al., 2012). Moreover, these results raise the possibility that this behavior of PCH-2 and/or meiotic HORMADs might be regulated by post-translational modifications associated with crossover control, such as ubiquitination, SUMOylation and phosphorylation (Gray & Cohen, 2016).

Given that mutation of PCH-2 produces changes in the number and distribution of crossovers across multiple model systems, we argue that controlling crossover distribution and number is the conserved role of PCH-2 in meiosis (Bhalla, 2023). We have previously proposed that the conserved role of PCH-2 is to coordinate meiotic recombination with synapsis (Bhalla, 2023). With these results, we further refine this model. Early in meiotic prophase, PCH-2 remodels meiotic HORMADs to prevent some DSBs from becoming crossover-eligible intermediates, widening the recombination landscape beyond early homolog interactions and/or sites that tend to be more favorable for DSB formation, also known as 'hot spots." For example, this may explain the localization of TRIP13, the PCH-2 ortholog in mice, to telomeres (Chotiner et al., 2024), sites that experience early homolog interactions due to the organization of meiotic chromosomes in the bouquet formation (Scherthan et al., 1996). This antagonism may also expand the regions of the genome that initiate synapsis in organisms that use

DSBs to accomplish this event. This possibility is supported by the observation that loss of TRIP13 in mammals produce meiotic chromosomes that exhibit partial asynapsis (Roig et al., 2010), particularly near regions that may act as barriers to SC polymerization (Brown et al., 2005; Roig et al., 2010). Limiting which DSBs becomes crossover-eligible intermediates in early meiotic prophase also ensures that meiotic recombination overlaps with synapsis, either completely, as in *C. elegans* (Yokoo et al., 2012) or partially, as in budding yeast, plants and mice (Capilla-Perez et al., 2021; Cole et al., 2012; Joshi et al., 2015; Morgan et al., 2021). Once synapsis is complete, PCH-2 continues to remodel meiotic HORMADs on chromosomes to control the gradual implementation of crossover number and distribution, reinforcing the important role that synapsis plays in mediating crossover control (Durand et al., 2022; Libuda et al., 2013).

Unexpectedly, the inability to reduce the number of crossover-eligible intermediates in *pch-2* mutants, as visualized by GFP::MSH-5 foci, does not produce extra crossovers but a loss of crossover-assurance in *C. elegans* (Figure 4), a somewhat counterintuitive result. One interpretation of these data is that crossover-eligible intermediates may be more numerous but absent from some chromosomes in *pch-2* mutants, explaining the loss of crossover assurance. Since the absence of crossover intermediates in *C. elegans* is accompanied by premature desynapsis of individual chromosomes (Machovina et al., 2016; Pattabiraman et al., 2017) and chromosomes in *pch-2* mutants delay desynapsis (Deshong et al., 2014), we do not favor this interpretation. Instead, we propose that having too many crossover-eligible intermediates can be as deleterious to crossover assurance as having too few (Figure 7B). This possibility is further supported by the loss of crossover assurance we detect in irradiated wildtype worms, which is exacerbated in *pch-2* mutants (Figure 2).

This phenomenon, where crossover-eligible intermediates need to be winnowed to some threshold number to ensure crossover assurance, may also explain the loss of crossover assurance also observed in *Trip13* deficient mice (Roig et al., 2010) and on small chromosomes in budding yeast

(Chakraborty et al., 2017). Alternatively, the counterintuitive relationship between the number of crossover-eligible precursors and crossover assurance in *pch-2* mutants we observe might reflect an additional layer of regulation during crossover formation specific to *C. elegans*. Since *C. elegans* chromosomes are holocentric, crossovers play an additional role organizing chromosomes for the ordered release of sister chromatid cohesion during meiosis I (Martinez-Perez et al., 2008; Nabeshima et al., 2005) and extra crossovers can be deleterious to accurate chromosome segregation (Hollis et al., 2020). By contrast, in *Arabidopsis*, a system that appears to be able to tolerate an extraordinarily high number of crossovers with little to no effect on chromosome segregation (Durand et al., 2022), PCH2's inability to localize to the SC produces an increase in crossover formation (Figure 7), as visualized by both MLH1 foci and the formation of chiasmata (Yang et al., 2022). Once again, an overarching theme that becomes apparent in our model is that PCH-2 may play a common role in different systems, with dramatic variations in phenotypic consequences given species-specific requirements and constraints.

We were not surprised to see high numbers of double crossovers on almost every chromosome in our genetic analysis of recombination in wildtype worms, given our previous analysis (Deshong et al., 2014). However, we were surprised to see that the majority of them were found near Pairing Centers and sites of synapsis initiation, suggesting a relationship between early homolog interactions and the formation of double crossovers. When we revisited our previous data, we observed similar patterns. In addition, we do not detect these double crossovers cytologically in *C. elegans*, even when using the OLLAS::COSA-1 reporter, which has been reported to identify double crossovers in spermatogenesis not visualized by GFP::COSA-1 (Cahoon et al., 2023). Crossovers that are cytologically marked by COSA-1 are known as Class I crossovers, which depend on pro-crossover factors such as MSH-5 and ZHP-3, and exhibit crossover control (Gray & Cohen, 2016). These data raise the intriguing possibility that these double crossovers are the product of the alternate, Class II, pathway of crossover formation, which relies on a different suite of proteins, does not respond to crossover control and

contributes to varying degrees in different model systems (Gray & Cohen, 2016; Youds et al., 2010). Thus, important corollaries of our model may be that PCH-2 specifically coordinates recombination with synapsis to promote Class I crossovers, limit Class II crossovers and that Class II crossovers are more likely to form early in meiosis, prior to synapsis. Therefore, variations in the contribution of the Class II crossover pathways to crossover recombination and the degree of cross-talk between Class I and Class II pathways among model systems might reflect the degree to which crossover formation overlaps with synapsis (Bhalla, 2023; Gray & Cohen, 2016; Yokoo et al., 2012). Furthermore, these corollaries are entirely consistent with PCH-2's absence from the genome of fission yeast (Wu & Burgess, 2007), a system in which chromosomes do not undergo synapsis, crossovers do not exhibit interference and all crossovers are dependent on the Class II pathway (Hollingsworth & Brill, 2004).

Our results also have some additional important implications about the regulation of DSB formation across the genome in *C. elegans*. We explain the shift in the recombination landscape away from the central regions of chromosomes and toward PC ends in *pch-2* mutants (Figure 1) as a result of early DSBs becoming crossovers at the expense of later DSBs, suggesting that when DSBs happen in meiotic prophase affects where they happen in the genome. Specifically, we propose that chromosome arms, which are gene poor, receive DSBs early during (or even throughout) DSB formation and the center of chromosomes, which are gene rich, receive DSBs later. A similar regulation of the timing of DSB formation has been demonstrated in budding yeast, where the DSB landscape across the whole genome expands when time in prophase is increased (López Ruiz et al., 2024) and small, highly recombinogenic, chromosomes, get more DSBs later in meiotic prophase (Murakami et al., 2020; Subramanian et al., 2019). However, this temporal regulation has not been reported previously in *C. elegans* and suggests that this phenomenon is more widely conserved. This expansion of the DSB landscape in *C. elegans* to include the center regions of chromosomes later in meiosis may be a deliberate attempt for recombination to create new haplotypes for evolution to act on, despite the relative paucity of DSBs and the observation that they can result in chromosome missegregation (Altendorfer et al., 2020).

Finally, our work raises some important questions about the functional role(s) of DSBs in meiosis, aside from their contributions to crossover formation. Hicks and colleagues were the first to report that early DSBs do not contribute to crossover formation in *C. elegans* (Hicks et al., 2022). Here we show that these early DSBs are prevented from becoming crossovers by both PCH-2 activity and cell cycle stage, specifically in leptotene/zygotene, when homologs are initiating pairing and synapsis. In budding yeast, similar, early-occurring DSBs have been characterized as “scout DSBs” because of their preference for repair from sister chromatids, versus homologous chromosomes, and their proposed role in contributing to homolog pairing (Borde & de Massy, 2015; Joshi et al., 2015). The homolog bias that these “scout DSBs” do display seems dependent on budding yeast *PCH2* (Joshi et al., 2015) but interpreting this experiment is complicated by the fact that Pch2 is also required to make the budding yeast meiotic HORMAD, Hop1, available for its loading onto meiotic chromosomes (Herruzo et al., 2021).

In contrast to budding yeast, *C. elegans* does not rely on DSBs to promote homolog pairing and initiate synapsis (Dernburg et al., 1998); in worms, *cis*-acting sites called Pairing Centers are essential for homolog pairing and synapsis (MacQueen et al., 2005). There is certainly some support in the literature for DSBs playing a role in supporting pairing and synapsis in *C. elegans* (Guo et al., 2022; Mlynarczyk-Evans et al., 2013; Roelens et al., 2015). However, if these early DSBs were contributing to pairing and synapsis, we would expect to see a genetic interaction between *htp-3*^{H96Y} and *pch-2* mutations in the installation of GFP::MSH-5 in the transition zone; we previously reported that *htp-3*^{H96Y} suppresses the acceleration of pairing and synapsis of *pch-2* mutants, particularly when Pairing Center function is compromised (Russo et al., 2023). Instead, we favor the possibility that these early DSBs are generated to amplify the signaling of DNA damage kinases to prime them for their role in recombination, a role that has also been proposed for “scout” DSBs (Joshi et al., 2015). That ATM-1, a conserved DNA damage kinase that is downstream of CHK-2 in *C. elegans*, relies on DSBs for full activity, supports this proposed, conserved role (Yu et al., 2023).

Our work provides an important framework to finally understand the role of PCH-2 in controlling the number and distribution of crossovers, a role that we argue is its conserved role. While specific details may vary across systems, we propose that PCH-2 remodels meiotic HORMADs throughout meiotic prophase to destabilize crossover-eligible precursors, coordinating meiotic recombination with synapsis, contributing to the progressive implementation of meiotic recombination and guaranteeing crossover assurance, interference and homeostasis.

Methods and Materials

C.elegans Genetics and Genome Engineering

The *C. elegans* Bristol N2 was used as the wild-type strain. All strains were maintained at 20ºC under standard conditions unless stated. Mutant combinations were generated by crossing. The following mutants and rearrangements were used:

LGII: pch-2(tm1458), meIs8 ([pie-1p::GFP::cosa-1 + unc-119(+)], dsb-2(me96), dsb-2(ie58[dsb-2::AID::3xFLAG])

LGIII: cosa-1(ddr12[OLLAS::cosa-1]); htp-3(vc75)

LGIV: him-3(blt9), spo-11(ie59[spo-11::AID::3xFLAG]), msh-5[ddr22(GFP::msh-5)], ieSi38 [sun-1p::TIR1::mRuby::sun-1 3'UTR + Cbr-unc-119(+)]

LGV: syp-1(icm85[T452A]), nT1[qIs51], bcIs39 (Plin-15::ced-1::GFP)

Genetic analysis of Recombination

The wildtype Hawaiian CB4856 strain (HI) and the Bristol N2 strain were used to assay recombination between single nucleotide polymorphisms (SNPs) on Chromosomes I, III, IV and X (Wicks et al., 2001; Bazan et al., 2011). The SNPs, primers, enzymes used for restriction digests and expected fragment sizes are included in Supplemental Table 1. To measure wild-type recombination, N2 males containing *bcIs39* were crossed to Hawaiian CB4856 worms. Cross-progeny hermaphrodites were identified by the presence of *bcIs39* and contained one N2 and one CB4856 chromosome.

These were assayed for recombination by crossing with CB4856 males containing *myo-2::mCherry*. Cross-progeny hermaphrodites from the resulting cross were isolated as L4s, and then cultured individually in 96- well plates in liquid S-media complete supplemented with HB101. Four days after initial culturing, starved populations were lysed and used for PCR and restriction digest to detect N2 and CB4856 SNP alleles. For recombination in *pch-2* mutants, strains homozygous for the CB4856 background of the relevant SNPs were created, then mated with *pch-2; bcIs39*. Subsequent steps were performed as in the wild-type worms.

Immunostaining

DAPI staining and immunostaining was performed as in (Russo et al. 2023), 20 to 24 hours post L4 unless otherwise noted. For analyzing bivalents, the same protocol was implemented with the exception that hermaphrodites were dissected and DAPI stained 48 hours post late L4 stage, unless otherwise noted.

The following primary antibodies were used at the indicated dilutions: alpaca anti-GFP Booster (ChromoTek, gb2AF488) was used at 1:1000; rat anti-OLLAS (Invitrogen, PIMA516125) was used at 1:1000; and rabbit anti PCH-2 (Bhalla 2014) was used at 1:500. The following secondary antibodies were used at the indicated dilutions: anti-rabbit Cy3 (Jackson Labs) was used at 1:500 and anti-rat Cy5 (Jackson Labs) was used at 1:500

Irradiation Experiments

Control and *pch-2* mutant L4's were aged 12-14 hours before being exposed to 1,000 rad (10 Gy) of X-ray radiation using a Precision MultiRad 160 X-irradiator (Precision X-Ray Inc.). Germlines were then fixed and stained, 8 hours and 24 hours post irradiation.

Auxin-induced Degradation Experiments

Auxin treatment was performed by transferring young adult worms (aged 12-14 hours post-L4) to bacteria-seeded plates containing auxin or 99% ethanol at specific time points, except for experiments in which L4s were transferred directly to bacteria-seeded plates containing auxin or ethanol (the 36 hour and 48 hour time points in Figures 3C and E and the experiments in Figures 5C and D). The natural auxin indole3-acetic acid (IAA) was purchased from Alfa Aesar (#A10556). A 400 mM stock solution in ethanol was prepared and was stored at 4ºC for up to one month. Auxin was diluted to 100mM, and 100ul was spread onto NGM plates. Plates were allowed to dry before seeding with fresh OP50 culture. Plates were left at 20ºC for 2-3 days in the dark to allow for bacterial lawn growth.

Imaging and Quantification

All images were acquired using a DeltaVision Personal DV system (Applied Precision) equipped with a 100X N.A. 1.40 oil-immersion objective (Olympus), resulting in an effective XY pixel spacing of 0.064 or 0.040 µm. Three-dimensional image stacks were collected at 0.2-µm Z spacing and processed by constrained, iterative deconvolution. Image scaling, analysis and maximum-intensity projections were performed using functions in the softWoRx software package.

For analysis of GFP::MSH-5 foci, sum projections were generated using ImageJ for each image of the germline. ImageJ plugins Cell Counter, ROI Manager, and Find Maxima were used to identify and quantify GFP::MSH-5 foci by row from transition zone to the end of pachytene. The threshold value was set depending on background conditions to ensure minimal signals were identified. Foci were

only quantified if they co-localized with DAPI staining. For all genotypes, three germlines per genotype were analyzed and representative germlines are shown.

Graphing and Statistical Analysis

Data was analyzed using Python 3.8 and Prism for statistical significance. All datasets were tested for normality using the Shapiro-Wilk test. For Figures 1, 2 and 5B, Fisher's exact test was used to determine significance. For Figures 3, 4, 5D and 6, Mann-Whitney U test was used to determine significance.

Author contributions

B.P., M.G., and N.B. designed the experiments. B.P., M.G., A.H., E.L., and V.O. performed the experiments. B.P. and N.B. analyzed the data. B.P. and N.B. wrote the initial draft of the manuscript and B.P., M.G., A.H. and N.B. revised the manuscript. N.B. acquired funding.

Acknowledgements

We would like to thank Josh Arribere, Pete Carlton, Abby Dernburg, Nicola Silva and Anne Villeneuve for valuable strains and reagents. We would also like to thank the members of the Bhalla lab for careful review of the manuscript. This work was supported by the NIH (grant numbers R35GM141835 [N.B.], R25GM051765 [V.O.] and T34GM140956 (A.H. and V.O.). Some strains were provided by the CGC, which is funded by NIH Office of Research Infrastructure Programs (P40 OD010440).

References

Altendorfer, E., Láscarez-Lagunas, L. I., Nadarajan, S., Mathieson, I., & Colaiácovo, M. P. (2020). Crossover Position Drives Chromosome Remodeling for Accurate Meiotic Chromosome Segregation. *Current Biology*, 30(7), 1329-1338.e7. https://doi.org/10.1016/j.cub.2020.01.079

Baudrimont, A., Paouneskou, D., Mohammad, A., Lichtenberger, R., Blundon, J., Kim, Y., Hartl, M., Falk, S., Schedl, T., & Jantsch, V. (2022). Release of CHK-2 from PPM-1.D anchorage schedules meiotic entry. *Science Advances*, 8(7), eabl8861. https://doi.org/10.1126/sciadv.abl8861

Bhalla, N. (2023). PCH-2 and meiotic HORMADs: A module for evolutionary innovation in meiosis? *In Current Topics in Developmental Biology* (Vol. 151, pp. 317–344). Elsevier. https://doi.org/10.1016/bs.ctdb.2022.07.001

Borde, V., & deMassy, B. (2015). Meiosis: Early DNA Double-Strand Breaks Pave the Way for Inter-Homolog Repair. *Developmental Cell*, 32(6), 663–664. https://doi.org/10.1016/j.devcel.2015.03.011

Börner, G. V., Barot, A., & Kleckner, N. (2008). Yeast Pch2 promotes domainal axis organization, timely recombination progression, and arrest of defective recombinosomes during meiosis. *Proceedings of the National Academy of Sciences*, 105(9), 3327–3332. https://doi.org/10.1073/pnas.0711864105

Brandt, J. N., Hussey, K. A., & Kim, Y. (2020). Spatial and temporal control of targeting Polo-like kinase during meiotic prophase. *Journal of Cell Biology*, 219(11), e202006094. https://doi.org/10.1083/jcb.202006094

Brown, P. W., Judis, L., Chan, E. R., Schwartz, S., Seftel, A., Thomas, A., & Hassold, T. J. (2005). Meiotic Synapsis Proceeds from a Limited Number of Subtelomeric Sites in the Human Male. *The American Journal of Human Genetics*, 77(4), 556–566. https://doi.org/10.1086/468188

Cahoon CK, Uebel CJ, Villeneuve AM, Libuda DE. Epitope tag-specific differences in the detection of COSA-1 marked crossover sites in *C. elegans* spermatocytes. *MicroPubl Biol.* 2023 Jan 6;2023:10.17912/micropub.biology.000724. https://doi.org/10.17912/micropub.biology.000724.

Capilla-Pérez, L., Durand, S., Hurel, A., Lian, Q., Chambon, A., Taochy, C., Solier, V., Grelon, M., & Mercier, R. (2021). The synaptonemal complex imposes crossover interference and heterochiasmy in Arabidopsis. *Proceedings of the National Academy of Sciences*, 118(12), e2023613118. https://doi.org/10.1073/pnas.2023613118

Castellano-Pozo, M., Pacheco, S., Sioutas, G., Jaso-Tamame, A. L., Dore, M. H., Karimi, M. M., & Martinez-Perez, E. (2020). Surveillance of cohesin-supported chromosome structure controls meiotic progression. *Nature Communications*, 11(1), 4345. https://doi.org/10.1038/s41467-020-18219-9

Chakraborty, P., Pankajam, A. V., Lin, G., Dutta, A., Krishnaprasad, G. N., Tekkedil, M. M., Shinohara, A., Steinmetz, L. M., & Nishant, K. T. (2017). Modulating Crossover Frequency and Interference for Obligate Crossovers in Saccharomyces cerevisiae Meiosis. *Genes|Genomes|Genetics*, 7(5), 1511–1524. https://doi.org/10.1534/g3.117.040071

Chotiner, J. Y., Leu, N. A., Yang, F., Cossu, I. G., Guan, Y., Lin, H., & Wang, P. J. (2024). TRIP13 localizes to synapsed chromosomes and functions as a dosage-sensitive regulator of meiosis. https://doi.org/10.7554/eLife.92195.2

Chu, L., Zhuang, J., Geng, M., Zhang, Y., Zhu, J., Zhang, C., Schnittger, A., Yi, B., & Yang, C. (2024). ASYNAPSIS3 has diverse dosage-dependent effects on meiotic crossover formation in Brassica napus. *The Plant Cell*, koae207. https://doi.org/10.1093/plcell/koae207

Cole, F., Kauppi, L., Lange, J., Roig, I., Wang, R., Keeney, S., & Jasin, M. (2012). Homeostatic control of recombination is implemented progressively in mouse meiosis. *Nature Cell Biology*, 14(4), 424–430. https://doi.org/10.1038/ncb2451

Couteau, F., Nabeshima, K., Villeneuve, A., & Zetka, M. (2004). A Component of *C. elegans* Meiotic Chromosome Axes at the Interface of Homolog Alignment, Synapsis, Nuclear Reorganization, and Recombination. *Current Biology*, 14(7), 585–592. https://doi.org/10.1016/j.cub.2004.03.033

Couteau, F., & Zetka, M. (2005). HTP-1 coordinates synaptonemal complex assembly with homolog alignment during meiosis in *C. elegans*. *Genes & Development*, 19(22), 2744–2756. https://doi.org/10.1101/gad.1348205

Cuacos, M., Lambing, C., Pachon-Penalba, M., Osman, K., Armstrong, S. J., Henderson, I. R., Sanchez-Moran, E., Franklin, F. C. H., & Heckmann, S. (2021). Meiotic chromosome axis remodelling is critical for meiotic recombination in *Brassica rapa*. *Journal of Experimental Botany*, 72(8), 3012–3027. https://doi.org/10.1093/jxb/erab035

Dernburg, A. F., McDonald, K., Moulder, G., Barstead, R., Dresser, M., & Villeneuve, A. M. (1998). Meiotic Recombination in *C. elegans* Initiates by a Conserved Mechanism and Is Dispensable for Homologous Chromosome Synapsis. *Cell*, 94(3), 387–398. https://doi.org/10.1016/S0092-8674(00)81481-6

Deshong, A. J., Ye, A. L., Lamelza, P., & Bhalla, N. (2014). A Quality Control Mechanism Coordinates Meiotic Prophase Events to Promote Crossover Assurance. *PLoS Genetics*, 10(4), e1004291. https://doi.org/10.1371/journal.pgen.1004291

Durand, S., Lian, Q., Jing, J., Ernst, M., Grelon, M., Zwicker, D., & Mercier, R. (2022). Joint control of meiotic crossover patterning by the synaptonemal complex and HEI10 dosage. *Nature Communications*, 13(1), 5999. https://doi.org/10.1038/s41467-022-33472-w

Girard, C., Zwicker, D., & Mercier, R. (2023). The regulation of meiotic crossover distribution: A coarse solution to a century-old mystery? *Biochemical Society Transactions*, 51(3), 1179–1190. https://doi.org/10.1042/BST20221329

Goodyer, W., Kaitna, S., Couteau, F., Ward, J. D., Boulton, S. J., & Zetka, M. (2008). HTP-3 Links DSB Formation with Homolog Pairing and Crossing Over during *C. elegans* Meiosis. *Developmental Cell*, 14(2), 263–274. https://doi.org/10.1016/j.devcel.2007.11.016

Gray, S., & Cohen, P. E. (2016). Control of Meiotic Crossovers: From Double-Strand Break Formation to Designation. *Annual Review of Genetics*, 50(1), 175–210. https://doi.org/10.1146/annurev-genet-120215-035111

Gu, Y., Desai, A., & Corbett, K. D. (2022). Evolutionary Dynamics and Molecular Mechanisms of HORMA Domain Protein Signaling. *Annual Review of Biochemistry*, 91(1), 541–569. https://doi.org/10.1146/annurev-biochem-090920-103246

Guo, H., Stamper, E. L., Sato-Carlton, A., Shimazoe, M. A., Li, X., Zhang, L., Stevens, L., Jacky Tam, K., Dernburg, A. F., & Carlton, P. M. (2022). Phosphoregulation of DSB-1 mediates control of meiotic double-strand break activity. *eLife*, 11, e77956. https://doi.org/10.7554/eLife.77956

Hassold, T., & Hunt, P. (2001). To err (meiotically) is human: The genesis of human aneuploidy. Nature Reviews *Genetics*, 2(4), 280–291. https://doi.org/10.1038/35066065

Haversat, J., Woglar, A., Klatt, K., Akerib, C. C., Roberts, V., Chen, S.-Y., Arur, S., Villeneuve, A. M., & Kim, Y. (2022). Robust designation of meiotic crossover sites by CDK-2 through phosphorylation of the MutSγ complex. *Proceedings of the National Academy of Sciences*, 119(21), e2117865119. https://doi.org/10.1073/pnas.2117865119

Herruzo, E., Lago-Maciel, A., Baztán, S., Santos, B., Carballo, J. A., & San-Segundo, P. A. (2021). Pch2 orchestrates the meiotic recombination checkpoint from the cytoplasm. *PLOS Genetics*, 17(7), e1009560. https://doi.org/10.1371/journal.pgen.1009560

Hicks, T., Trivedi, S., Eppert, M., Bowman, R., Tian, H., Dafalla, A., Crahan, C., Smolikove, S., & Silva, N. (2022). Continuous double-strand break induction and their differential processing sustain chiasma formation during *Caenorhabditis elegans* meiosis. *Cell Reports*, 40(13), 111403. https://doi.org/10.1016/j.celrep.2022.111403

Hollingsworth, N. M., & Brill, S. J. (2004). The Mus81 solution to resolution: Generating meiotic crossovers without Holliday junctions. *Genes & Development*, 18(2), 117–125. https://doi.org/10.1101/gad.1165904

Hollis, J. A., Glover, M. L., Schlientz, A. J., Cahoon, C. K., Bowerman, B., Wignall, S. M., & Libuda, D. E. (2020). Excess crossovers impede faithful meiotic chromosome segregation in *C. elegans*. *PLOS Genetics*, 16(9), e1009001. https://doi.org/10.1371/journal.pgen.1009001

Janisiw, E., Dello Stritto, M. R., Jantsch, V., & Silva, N. (2018). BRCA1-BARD1 associate with the synaptonemal complex and pro-crossover factors and influence RAD-51 dynamics during *Caenorhabditis elegans* meiosis. *PLOS Genetics*, 14(11), e1007653. https://doi.org/10.1371/journal.pgen.1007653

Jaramillo-Lambert, A., Ellefson, M., Villeneuve, A. M., & Engebrecht, J. (2007). Differential timing of S phases, X chromosome replication, and meiotic prophase in the *C. elegans* germ line. *Developmental Biology*, *308*(1), 206–221. https://doi.org/10.1016/j.ydbio.2007.05.019

Joshi, N., Barot, A., Jamison, C., & Börner, G. V. (2009). Pch2 Links Chromosome Axis Remodeling at Future Crossover Sites and Crossover Distribution during Yeast Meiosis. *PLOS Genetics*, 5(7), e1000557. https://doi.org/10.1371/journal.pgen.1000557

Joshi, N., Brown, M. S., Bishop, D. K., & Börner, G. V. (2015). Gradual Implementation of the Meiotic Recombination Program via Checkpoint Pathways Controlled by Global DSB Levels. *Molecular Cell*, 57(5), 797–811. https://doi.org/10.1016/j.molcel.2014.12.027

Joyce, E. F., & McKim, K. S. (2009). Drosophila PCH2 Is Required for a Pachytene Checkpoint That Monitors Double-Strand-Break-Independent Events Leading to Meiotic Crossover Formation. *Genetics*, 181(1), 39–51. https://doi.org/10.1534/genetics.108.093112

Keeney S, Giroux CN, Kleckner N. Meiosis-specific DNA double-strand breaks are catalyzed by Spo11, a member of a widely conserved protein family. *Cell*. 1997 Feb 7;88(3):375-84. doi: 10.1016/s0092-8674(00)81876-0. PMID: 9039264.

Kelly, K. O., Dernburg, A. F., Stanfield, G. M., & Villeneuve, A. M. (2000). *Caenorhabditis elegans* msh-5 Is Required for Both Normal and Radiation-Induced Meiotic Crossing Over but Not for Completion of Meiosis. *Genetics*, 156(2), 617–630. https://doi.org/10.1093/genetics/156.2.617

Kim, Y., Kostow, N., & Dernburg, A. F. (2015). The Chromosome Axis Mediates Feedback Control of CHK-2 to Ensure Crossover Formation in *C. elegans*. *Developmental Cell*, 35(2), 247–261. https://doi.org/10.1016/j.devcel.2015.09.021

Kim, Y., Rosenberg, S. C., Kugel, C. L., Kostow, N., Rog, O., Davydov, V., Su, T. Y., Dernburg, A. F., & Corbett, K. D. (2014). The Chromosome Axis Controls Meiotic Events through a Hierarchical Assembly of HORMA Domain Proteins. *Developmental Cell*, 31(4), 487–502. https://doi.org/10.1016/j.devcel.2014.09.013

Lambing, C., Kuo, P. C., Tock, A. J., Topp, S. D., & Henderson, I. R. (2020). ASY1 acts as a dosage-dependent antagonist of telomere-led recombination and mediates crossover interference in *Arabidopsis*. *Proceedings of the National Academy of Sciences*, 117(24), 13647–13658. https://doi.org/10.1073/pnas.1921055117

Lambing, C., Osman, K., Nuntasoontorn, K., West, A., Higgins, J. D., Copenhaver, G. P., Yang, J., Armstrong, S. J., Mechtler, K., Roitinger, E., & Franklin, F. C. H. (2015). *Arabidopsis* PCH2 Mediates Meiotic Chromosome Remodeling and Maturation of Crossovers. *PLOS Genetics*, 11(7), e1005372. https://doi.org/10.1371/journal.pgen.1005372

Libuda, D. E., Uzawa, S., Meyer, B. J., & Villeneuve, A. M. (2013). Meiotic chromosome structures constrain and respond to designation of crossover sites. *Nature*, 502(7473), 703–706. https://doi.org/10.1038/nature12577

López Ruiz, L. M., Johnson, D., Gittens, W. H., Brown, G. G. B., Allison, R. M., & Neale, M. J. (2024). Meiotic prophase length modulates Tel1-dependent DNA double-strand break interference. PLOS *Genetics*, 20(3), e1011140. https://doi.org/10.1371/journal.pgen.1011140

Machovina, T. S., Mainpal, R., Daryabeigi, A., McGovern, O., Paouneskou, D., Labella, S., Zetka, M., Jantsch, V., Yanowitz, J. L. (2016). A Surveillance System Ensures Crossover Formation in *C. elegans*. *Current Biology*, 26(21), 2873-2884. https://doi.org/10.1016/j.cub.2016.09.007

MacQueen, A. J., Phillips, C. M., Bhalla, N., Weiser, P., Villeneuve, A. M., & Dernburg, A. F. (2005). Chromosome Sites Play Dual Roles to Establish Homologous Synapsis during Meiosis in *C. elegans*. *Cell*, 123(6), 1037–1050. https://doi.org/10.1016/j.cell.2005.09.034

MacQueen, A. J., & Villeneuve, A. M. (2001). Nuclear reorganization and homologous chromosome pairing during meiotic prophase require *C. elegans chk-2*. *Genes & Development*, 15(13), 1674–1687. https://doi.org/10.1101/gad.902601

Martinez-Perez, E., Schvarzstein, M., Barroso, C., Lightfoot, J., Dernburg, A. F., & Villeneuve, A. M. (2008). Crossovers trigger a remodeling of meiotic chromosome axis composition that is linked to two-step loss of sister chromatid cohesion. *Genes & Development*, 22(20), 2886–2901. https://doi.org/10.1101/gad.1694108

Martinez-Perez, E., & Villeneuve, A. M. (2005). HTP-1-dependent constraints coordinate homolog pairing and synapsis and promote chiasma formation during *C. elegans* meiosis. *Genes & Development*, 19(22), 2727–2743. https://doi.org/10.1101/gad.1338505

Mlynarczyk-Evans, S., Roelens, B., & Villeneuve, A. M. (2013). Evidence That Masking of Synapsis Imperfections Counterbalances Quality Control to Promote Efficient Meiosis. *PLoS Genetics*, 9(12), e1003963. https://doi.org/10.1371/journal.pgen.1003963

Morgan, C., White, M. A., Franklin, F. C. H., Zickler, D., Kleckner, N., & Bomblies, K. (2021). Evolution of crossover interference enables stable autopolyploidy by ensuring pairwise partner connections in *Arabidopsis arenosa*. *Current Biology*, 31(21), 4713-4726.e4. https://doi.org/10.1016/j.cub.2021.08.028

Murakami, H., Lam, I., Huang, P.-C., Song, J., Van Overbeek, M., & Keeney, S. (2020). Multilayered mechanisms ensure that short chromosomes recombine in meiosis. *Nature*, 582(7810), 124–128. https://doi.org/10.1038/s41586-020-2248-2

Nabeshima, K., Villeneuve, A. M., & Colaiácovo, M. P. (2005). Crossing over is coupled to late meiotic prophase bivalent differentiation through asymmetric disassembly of the SC. *The Journal of Cell Biology*, 168(5), 683–689. https://doi.org/10.1083/jcb.200410144

Nabeshima, K., Villeneuve, A. M., & Hillers, K. J. (2004). Chromosome-Wide Regulation of Meiotic Crossover Formation in *Caenorhabditis elegans* Requires Properly Assembled Chromosome Axes. *Genetics*, 168(3), 1275–1292. https://doi.org/10.1534/genetics.104.030700

Nadarajan, S., Altendorfer, E., Saito, T. T., Martinez-Garcia, M., & Colaiácovo, M. P. (2021). HIM-17 regulates the position of recombination events and GSP-1/2 localization to establish short arm identity on bivalents in meiosis. *Proceedings of the National Academy of Sciences*, 118(17), e2016363118. https://doi.org/10.1073/pnas.2016363118

Patel, B; Grobler, M; Bhalla, N (2023). Chromosomal fusions, but not chromosomal inversions, activate a PCH-2 dependent checkpoint that promotes crossover formation in *C. elegans*. *microPublication Biology*.

Pattabiraman, D., Roelens, B., Woglar, A., Villeneuve A. M. (2017) Meiotic recombination modulates the structure and dynamics of the synaptonemal complex during *C. elegans* meiosis. *PLOS Genetics*, 13(3), e1006670. https://doi.org/10.1371/journal.pgen.1006670

Roelens, B., Schvarzstein, M., & Villeneuve, A. M. (2015). Manipulation of Karyotype in *Caenorhabditis elegans* Reveals Multiple Inputs Driving Pairwise Chromosome Synapsis During Meiosis. *Genetics*, 201(4), 1363–1379. https://doi.org/10.1534/genetics.115.182279

Roig, I., Dowdle, J. A., Toth, A., de Rooij, D. G., Jasin, M., & Keeney, S. (2010). Mouse TRIP13/PCH2 Is Required for Recombination and Normal Higher-Order Chromosome Structure during Meiosis. *PLOS Genetics,* 6(8), e1001062. https://doi.org/10.1371/journal.pgen.1001062

Rosu, S., Zawadzki, K. A., Stamper, E. L., Libuda, D. E., Reese, A. L., Dernburg, A. F., & Villeneuve, A. M. (2013). The *C. elegans* DSB-2 Protein Reveals a Regulatory Network that Controls Competence for Meiotic DSB Formation and Promotes Crossover Assurance. *PLOS Genetics*, 9(8), e1003674. https://doi.org/10.1371/journal.pgen.1003674

Russo, A. E., Giacopazzi, S., Deshong, A., Menon, M., Ortiz, V., Ego, K. M., Corbett, K. D., & Bhalla, N. (2023). The conserved AAA ATPase PCH-2 distributes its regulation of meiotic prophase events through multiple meiotic HORMADs in *C. elegans*. *PLOS Genetics*, 19(4), e1010708. https://doi.org/10.1371/journal.pgen.1010708

Sato-Carlton, A., Nakamura-Tabuchi, C., Chartrand, S. K., Uchino, T., & Carlton, P. M. (2018).

Phosphorylation of the synaptonemal complex protein SYP-1 promotes meiotic chromosome segregation. *Journal of Cell Biology*, 217(2), 555–570. https://doi.org/10.1083/jcb.201707161

Scherthan, H., Weich, S., Schwegler, H., Heyting, C., Härle, M., & Cremer, T. (1996). Centromere and telomere movements during early meiotic prophase of mouse and man are associated with the onset of chromosome pairing. *The Journal of Cell Biology*, 134(5), 1109–1125. https://doi.org/10.1083/jcb.134.5.1109

Snowden, T., Acharya, S., Butz, C., Berardini, M., & Fishel, R. (2004). hMSH4-hMSH5 Recognizes Holliday Junctions and Forms a Meiosis-Specific Sliding Clamp that Embraces Homologous Chromosomes. *Molecular Cell*, 15(3), 437–451. https://doi.org/10.1016/j.molcel.2004.06.040

Subramanian, V. V., Zhu, X., Markowitz, T. E., Vale-Silva, L. A., San-Segundo, P. A., Hollingsworth, N. M., Keeney, S., & Hochwagen, A. (2019). Persistent DNA-break potential near telomeres increases initiation of meiotic recombination on short chromosomes. *Nature Communications*, 10(1), 970. https://doi.org/10.1038/s41467-019-08875-x

Wicks, S. R., Yeh, R. T., Gish, W. R., Waterston, R. H., & Plasterk, R. H. A. (2001). Rapid gene mapping in *Caenorhabditis elegans* using a high density polymorphism map. *Nature Genetics*, 28(2), 160–164. https://doi.org/10.1038/88878

Woglar, A., & Villeneuve, A. M. (2018). Dynamic Architecture of DNA Repair Complexes and the Synaptonemal Complex at Sites of Meiotic Recombination. *Cell*, 173(7), 1678-1691.e16. https://doi.org/10.1016/j.cell.2018.03.066

Wojtasz, L., Daniel, K., Roig, I., Bolcun-Filas, E., Xu, H., Boonsanay, V., Eckmann, C. R., Cooke, H. J., Jasin, M., Keeney, S., McKay, M. J., & Toth, A. (2009). Mouse HORMAD1 and HORMAD2, Two

Conserved Meiotic Chromosomal Proteins, Are Depleted from Synapsed Chromosome Axes with the Help of TRIP13 AAA-ATPase. *PLOS Genetics*, 5(10), e1000702. https://doi.org/10.1371/journal.pgen.1000702

Wu, H. Y., & Burgess, S. M. (2006). Two distinct surveillance mechanisms monitor meiotic chromosome metabolism in budding yeast. *Current biology*: CB, 16(24), 2473–2479. https://doi.org/10.1016/j.cub.2006.10.069

Yang, C., Hu, B., Portheine, S. M., Chuenban, P., & Schnittger, A. (2020). State changes of the HORMA protein ASY1 are mediated by an interplay between its closure motif and PCH2. *Nucleic Acids Research*, 48(20), 11521-11535. https://doi.org/10.1093/nar/gkaa527

Yang, C., Sofroni, K., Hamamura, Y., Hu, B., Elbasi, H. T., Balboni, M., Chu, L., Stang, D., Heese, M., & Schnittger, A. (2022). ZYP1-mediated recruitment of PCH2 to the synaptonemal complex remodels the chromosome axis leading to crossover restriction. *Nucleic Acids Research*, 50(22), 12924–12937. https://doi.org/10.1093/nar/gkac1160

Yokoo, R., Zawadzki, K. A., Nabeshima, K., Drake, M., Arur, S., & Villeneuve, A. M. (2012). COSA-1 Reveals Robust Homeostasis and Separable Licensing and Reinforcement Steps Governing Meiotic Crossovers. *Cell*, 149(1), 75–87. https://doi.org/10.1016/j.cell.2012.01.052

Youds, J. L., Mets, D. G., McIlwraith, M. J., Martin, J. S., Ward, J. D., ONeil, N. J., Rose, A. M., West, S. C., Meyer, B. J., & Boulton, S. J. (2010). RTEL-1 Enforces Meiotic Crossover Interference and Homeostasis. *Science*, 327(5970), 1254–1258. https://doi.org/10.1126/science.1183112

Yu, Z., Kim, H. J., & Dernburg, A. F. (2023). ATM signaling modulates cohesin behavior in meiotic prophase and proliferating cells. *Nature Structural & Molecular Biology*, 30(4), 436–450. https://doi.org/10.1038/s41594-023-00929-5

Yu, Z., Kim, Y., & Dernburg, A. F. (2016). Meiotic recombination and the crossover assurance checkpoint in *Caenorhabditis elegans*. *Seminars in Cell & Developmental Biology*, 54, 106–116. https://doi.org/10.1016/j.semcdb.2016.03.014

Zanders, S., & Alani, E. (2009). The *pch2Δ* Mutation in Baker's Yeast Alters Meiotic Crossover Levels and Confers a Defect in Crossover Interference. *PLOS Genetics*, 5(7), e1000571. https://doi.org/10.1371/journal.pgen.1000571

Zhang, L., Köhler, S., Rillo-Bohn, R., & Dernburg, A. F. (2018). A compartmentalized signaling network mediates crossover control in meiosis. *eLife*, 7, e30789. https://doi.org/10.7554/eLife.30789

Zhang, L., Stauffer, W. T., Wang, J. S., Wu, F., Yu, Z., Liu, C., Kim, H. J., & Dernburg, A. F. (2023). Recruitment of Polo-like kinase couples synapsis to meiotic progression via inactivation of CHK-2. *eLife*, 12, e84492. https://doi.org/10.7554/eLife.84492

Zhang, L., Stauffer, W. T., Zwicker, D., & Dernburg, A. F. (2021). Crossover patterning through kinase-regulated condensation and coarsening of recombination nodules. [Preprint]. *bioRxiv*. https://doi.org/10.1101/2021.08.26.457865

Figure Legends

Figure 1. PCH-2 controls the number and distribution of crossovers in similar patterns on multiple chromosomes. Genetic analysis of meiotic recombination in wildtype and *pch-2* mutants. DCO indicates double crossovers. Physical and genetic maps of Chromosome I, III, IV and the X chromosome are depicted to scale. Genetic distance is shown in centimorgans. A * indicates a p-value < 0.05, a ** indicates a p value < 0.01 and a *** indicates p-value < 0.001.

Figure 2. PCH-2 prevents exogenous double strand breaks from becoming crossovers in early meiotic prophase. A. Illustration of the irradiation experiments in control and *pch-2* mutants. Box indicates late pachytene, the area where GFP::COSA-1 foci are analyzed. **B.** Meiotic nuclei in control animals and *pch-2* mutants 8 hours post irradiation stained for DAPI (magenta) and GFP::COSA-1 (green). Scale bar is 4 um. **C.** Fraction of meiotic nuclei with less than 6, 6, or greater than 6 GFP::COSA-1 foci in control animals(yellow) and *pch-2* mutants (blue) mutants 8 hours post irradiation. **D.** Meiotic nuclei in control animals and *pch-2* mutants 24 hours post irradiation with DAPI (magenta) and GFP::COSA-1 (green). **E.** Fraction of meiotic nuclei with less than 6, 6, or greater than 6 GFP::COSA-1 foci in control animals and *pch-2* mutants 24 hours post irradiation. A *** indicates p-value < 0.001, and a **** indicates p-value < 0.0001.

Figure 3. PCH-2 prevents SPO-11-induced double strand breaks from becoming crossovers in early meiotic prophase. A. Illustration of the SPO-11 depletion experiment to assay GFP::COSA-1 and bivalents in control animals and *pch-2* mutants at different timepoints of auxin treatment. Each timepoint indicates when SPO-11 is depleted in the germline with auxin induced degradation. Boxes indicate late pachytene, the area where GFP::COSA-1 foci are analyzed, and diakinesis, where bivalents are analyzed. **B.** Representative images of meiotic nuclei in control animals and *pch-2* mutants treated with auxin for 20 hours, stained for DAPI (magenta) and GFP::COSA-1 (green). Scale

bar is 5 um. **C.** Number of GFP::COSA-1 foci in meiotic nuclei at different timepoints of auxin treatment in control (blue) and *pch-2* mutants (yellow). Error bars represent standard error of the mean (SEM). **D.** Oocytes from control animals and *pch-2* mutants stained for DAPI (magenta). Scale bar is 4um. **E**. Number of DAPI stained bodies in meiotic nuclei at different timepoints of auxin treatment in control animals and *pch-2* mutants. Error bars represent SEM and a * indicates p-value < 0.05 and a *** indicates p-value < 0.001.

Figure 4. PCH-2 is required for timely loading and removal of MSH-5 on meiotic chromosomes through its regulation of HIM-3. A. Representative images of nuclei in different stages of meiotic prophase in control animals and *pch-2* mutants stained for DAPI (magenta) and GFP::MSH-5 (green) Scale bar is 5 um. **B.** Scatter plot showing average GFP::MSH-5 foci per row of germline nuclei in control animals (yellow) and *pch-2* mutants (blue) from the transition zone to late pachytene, normalized to 100. The line represents a rolling average of four rows. **C.** Representative images of nuclei in different stages of meiotic prophase in *him-3*^{R93Y} mutants (left) and *pch-2*;*him-3*^{R93Y} double mutants (right), stained for DAPI (magenta) and GFP::MSH-5 (green). **D.** Scatter plot showing average GFP::MSH-5 foci per row in *him-3*^{R93Y} (brown) and *pch-2;him-3*^{R93Y} mutants (pink) from the transition zone to late pachytene, normalized to 100. The line represents a rolling average of four rows. Similar data is provided for a control germline (opaque yellow) for comparison. **E.** Representative images of meiotic nuclei in control animals and *pch-2* mutants stained for DAPI (blue), GFP::MSH-5 (green), and OLLAS::COSA-1 (red). Yellow circles indicate GFP::MSH-5 without OLLAS::COSA-1. Scale bar is 4um. **F.** Scatter plot showing average GFP::MSH-5 (green) and OLLAS::COSA-1 (red) foci per row in the last five rows of the germline in control animals and *pch-2* mutants. The line represents a rolling average of 2 rows. **G.** Swarm plot showing number of GFP::MSH-5 foci in control (yellow) and *pch-2* mutant (blue) nuclei with less than 6 OLLAS::COSA-1 foci (left) and 6 OLLAS::COSA-1 foci (right). Error bars represent SEM. A * indicates a p-value less than 0.05 and a ** indicates a p-value < 0.01.

Figure 5. PCH-2 is removed when crossovers are designated. A. Representative images of meiotic nuclei in *dsb-2* animals 24 hours post L4 and 48 hours post L4 stained for DAPI (magenta), PCH-2 (red), and GFP::COSA-1 (green). Scale bar is 4 um. **B.** Stacked histograms showing percentage of PCH-2 positive and negative nuclei with (lime) and without (dark green) GFP::COSA-1 foci in *dsb-2* mutants at 24 hours post L4 and 48 hours post L4. **C.** Representative images of meiotic nuclei in *dsb-2::AID* and *dsb-2::AID;pch-2* mutants treated with auxin and stained for DAPI (magenta) and GFP::COSA-1 (green). Scale bar is 5 um. **D.** Swarm plot showing the number of GFP::COSA-1 foci in *dsb-2::AID* (gray) and *dsb-2::AID;pch-2* (lemon) mutants when treated with ethanol or auxin. Error bars represent the SEM. A ** indicates a p-value less than 0.01 and a **** indicates p-value < 0.0001.

Figure 6. PCH-2 and high CHK-2 activity control the fate of early double strand breaks. A. Illustration of CHK-2 activity in wildtype and *syp-1*^{T452A} germlines. **B.** Representative images of meiotic nuclei late pachytene in *syp-1*^{T452A} and *pch-2;syp-1*^{T452A} mutants stained for DAPI (magenta) and GFP::COSA-1 (green). Scale bar is 5 um. **C.** Swarm plot showing number of GFP::COSA-1 foci in control animals (blue), *pch-2* (yellow), *syp-1*^{T452A} (maroon), and *pch-2;syp-1*^{T452A} (light blue) mutants. Error bars represent SEM. **D.** Oocytes from *syp-1*^{T452A} and *pch-2;syp-1*^{T452A} mutant worms stained for DAPI (magenta). Scale bar is 4um. **D.** Swarm plot showing number of DAPI stained bodies in control animals (blue), *pch-2* (yellow), *syp-1*^{T452A} (maroon), and *pch-2;syp-1*^{T452A} (light blue) mutants. Error bars represent SEM. A **** indicates p-value < 0.0001.

Figure 7. PCH-2 remodels HIM-3 to disassemble crossover-eligible intermediates, controlling crossover distribution and number. A. Model for how *pch-2* and *him-3*^{R93Y} mutations genetically interact to affect the progression of meiotic recombination. HIM-3 adopts the closed conformation upon binding an interacting protein with a closure motif and its conversion to the extended conformation is facilitated by PCH-2's remodeling of its HORMA domain. **B.** Model for how PCH-2 and HIM-3 progressively implement meiotic recombination during different stages of meiotic prophase.

Supplemental Figure 1: PCH-2 does not regulate GFP::MSH-5 loading and removal through HTP-3. A. Representative images of nuclei in different stages of meiotic prophase in *htp-3*^{H96Y} and *pch-2; htp-3*^{H96Y} mutants stained for DAPI (magenta) and GFP::MSH-5 (green) Scale bar in all images is 5 um. **B.** Scatter plot showing average GFP::MSH-5 foci per row of germline nuclei in *htp-3*^{H96Y} (blue) and *pch-2; htp-3*^{H96Y} (green) mutants from the transition zone to late pachytene, normalized to 100. The line represents a rolling average of four rows.

Supplemental Figure 2: *pch-2* meiotic nuclei with elevated numbers of GFP::MSH-5 foci show defects in crossover assurance. Gray scale images of control and *pch-2* mutant nuclei stained for DAPI, GFP::MSH-5 and OLLAS::COSA-1. Scale bar in image is 4 um.

Figure 1

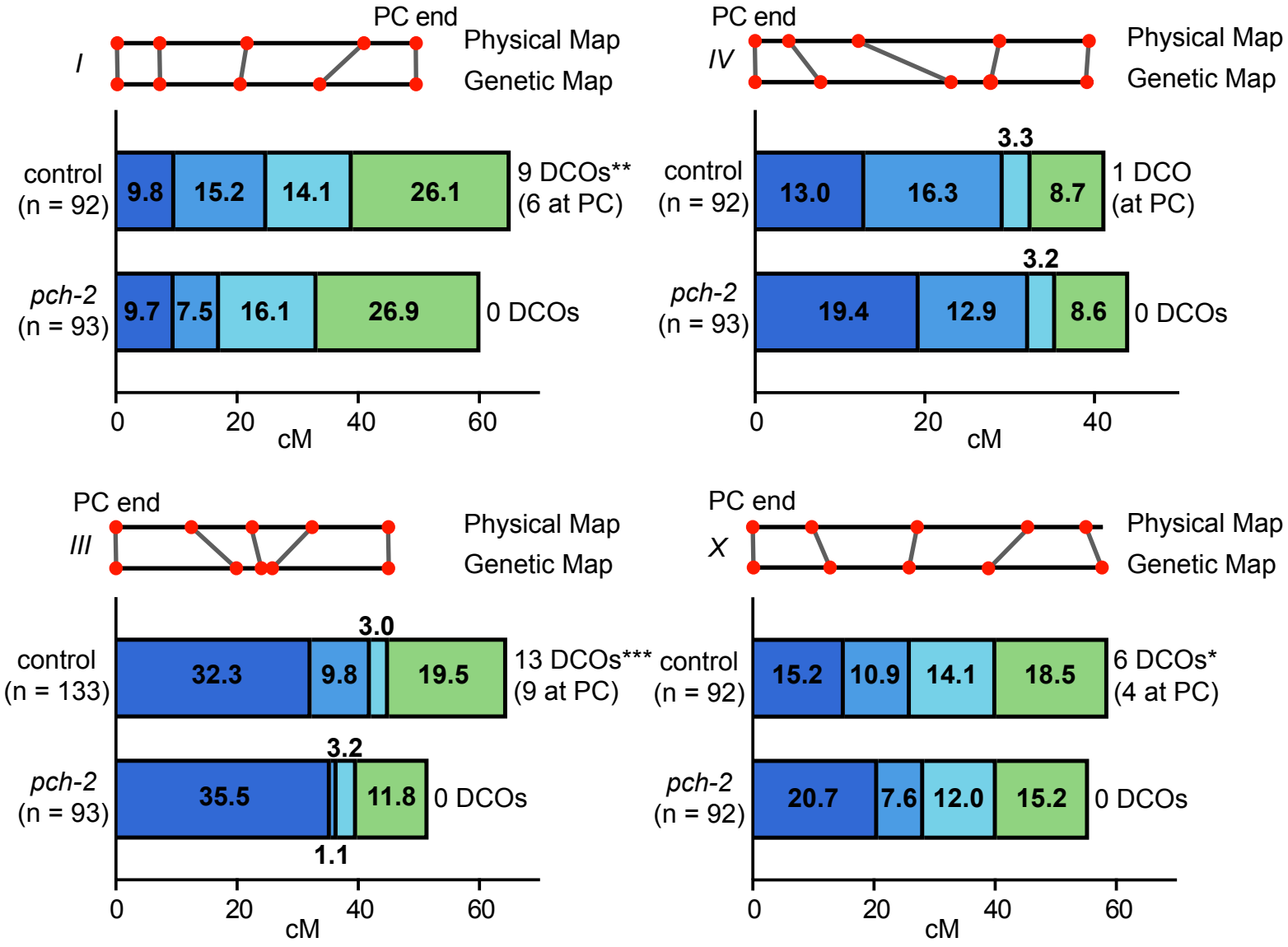
PC end
I
Physical Map
Genetic Map
control
(n = 92)
9.8
15.2
14.1
26.1
9 DCOs**
(6 at PC)
pch-2
(n = 93)
9.7
7.5
16.1
26.9
0 DCOs
0
20
40
60
cM
PC end
IV
Physical Map
Genetic Map
control
(n = 92)
13.0
16.3
3.3
8.7
1 DCO
(at PC)
pch-2
(n = 93)
19.4
12.9
3.2
8.6
0 DCOs
0
20
40
cM
PC end
III
Physical Map
Genetic Map
control
(n = 133)
32.3
9.8
3.0
19.5
13 DCOs***
(9 at PC)
pch-2
(n = 93)
35.5
1.1
3.2
11.8
0 DCOs
0
20
40
60
cM
PC end
X
Physical Map
Genetic Map
control
(n = 92)
15.2
10.9
14.1
18.5
6 DCOs*
(4 at PC)
pch-2
(n = 92)
20.7
7.6
12.0
15.2
0 DCOs
0
20
40
60
cM

Figure 2

A

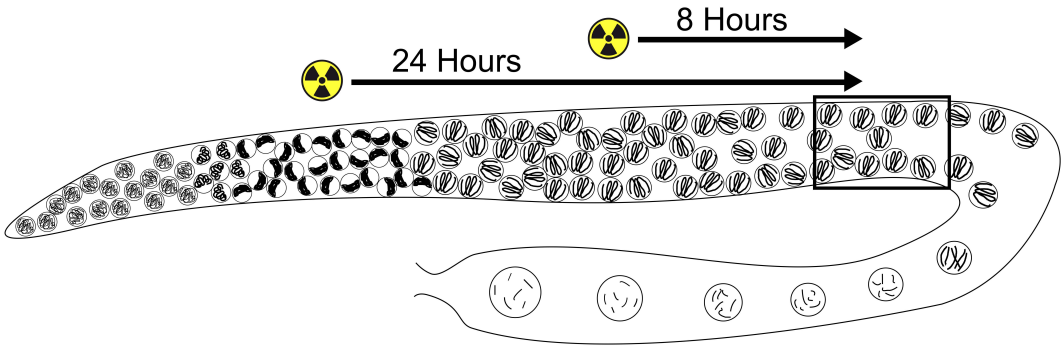

B

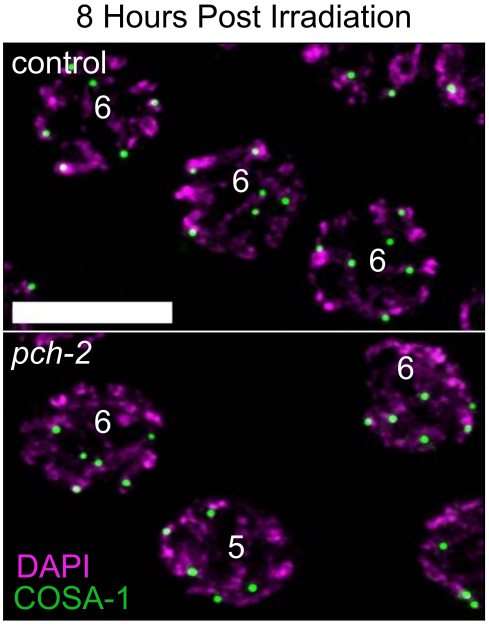

C

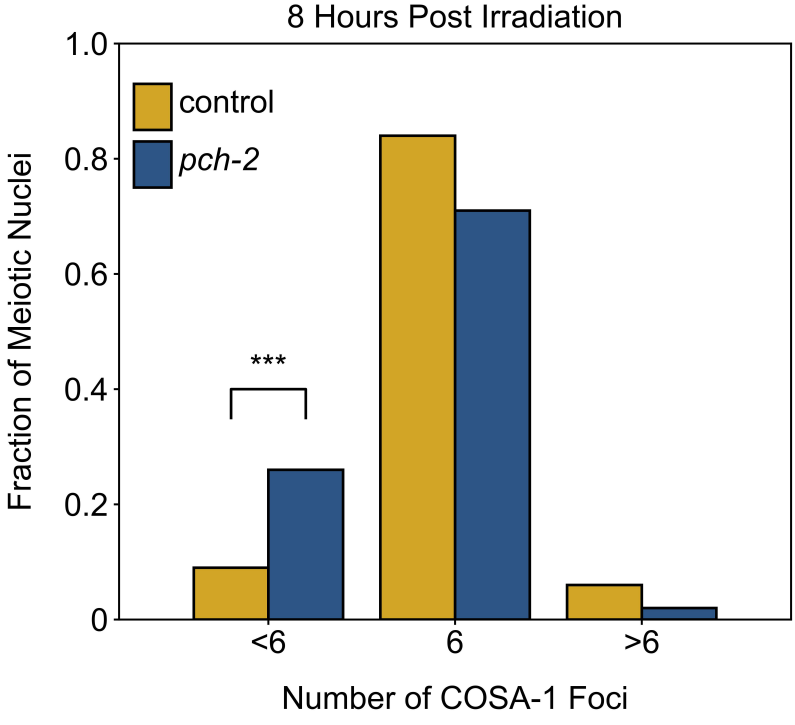

D

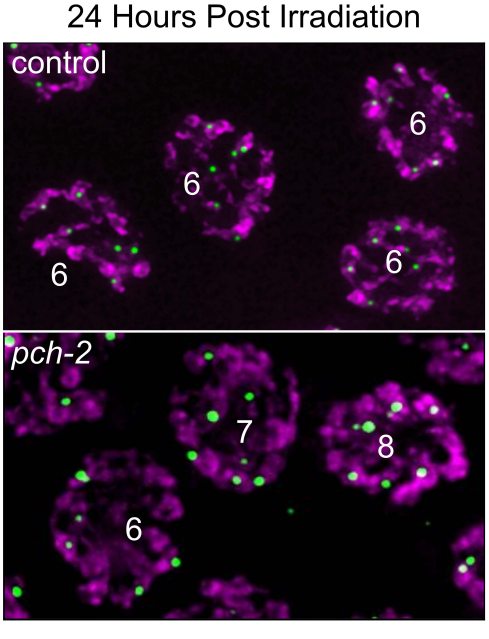

E

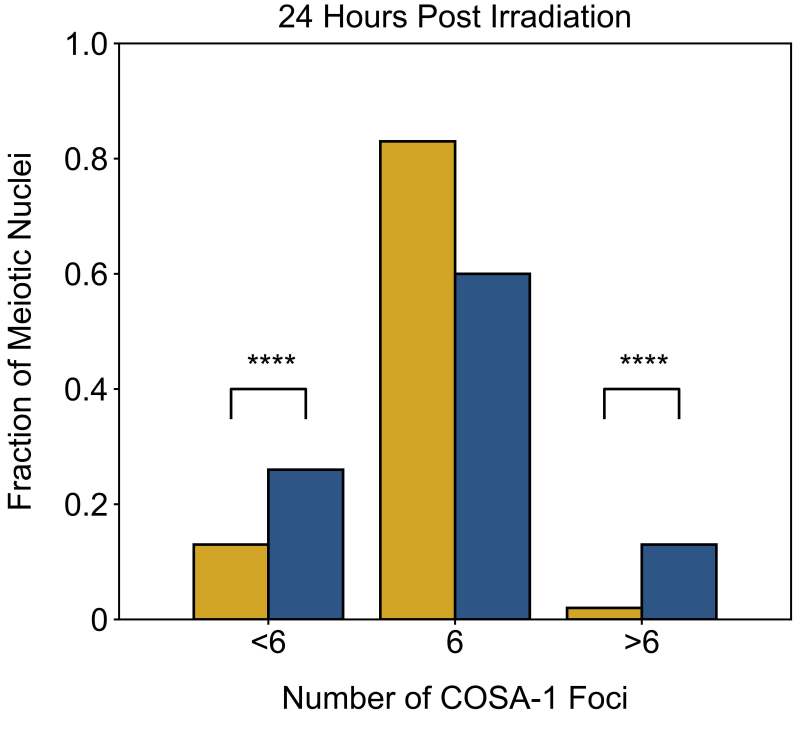

Figure 3

A

Areas of SPO-11 Depletion for COSA-1 and Bivalent Assay

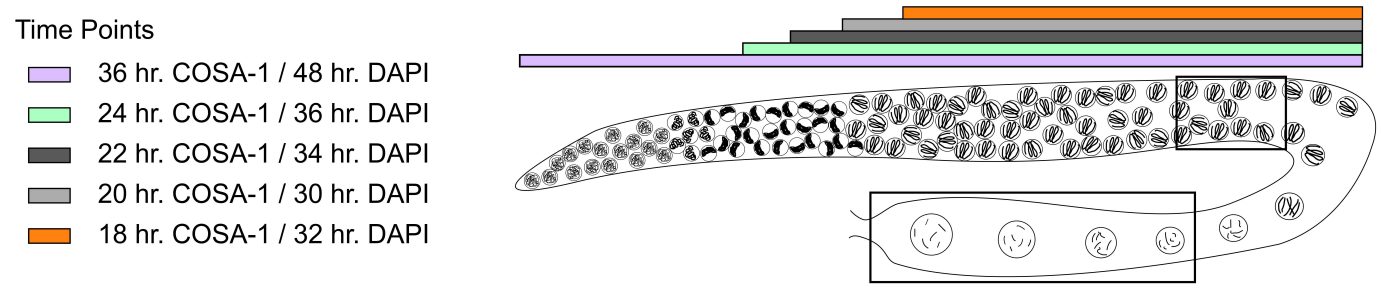

B

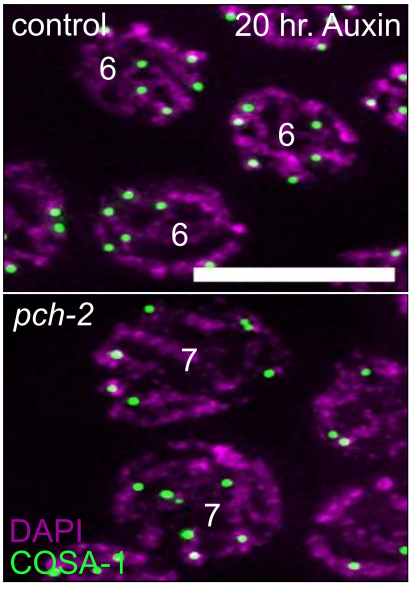

C

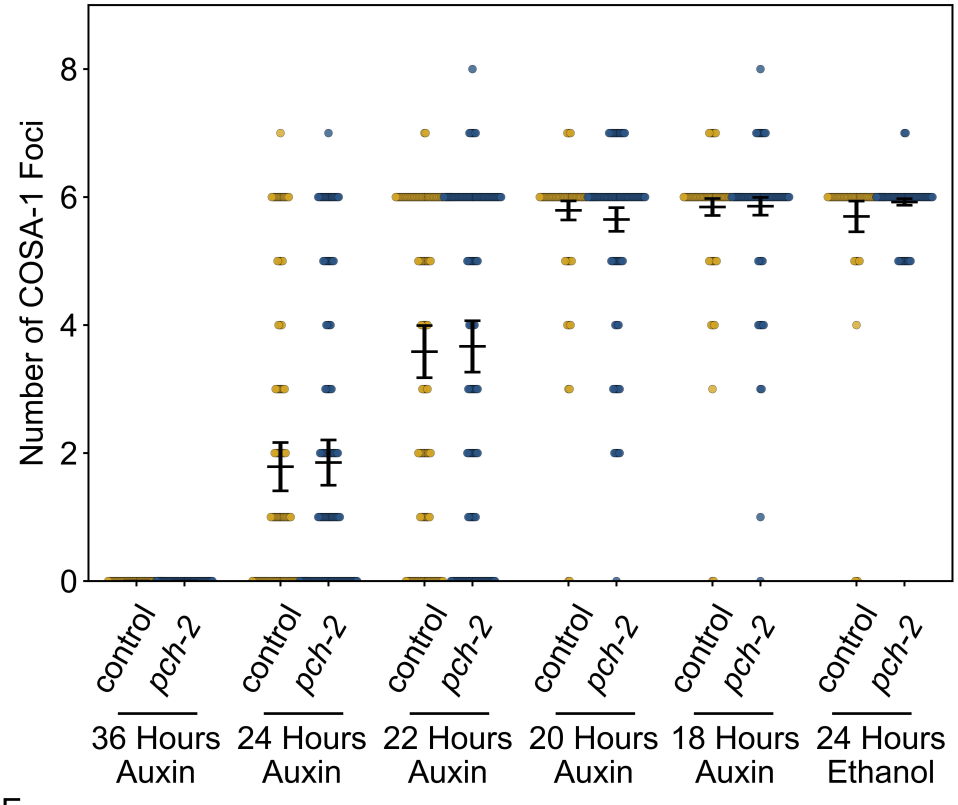

D

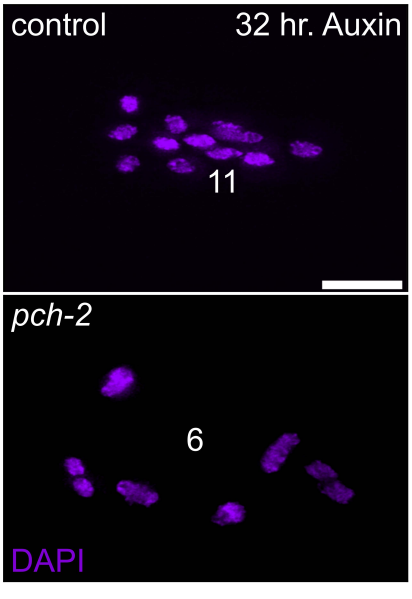

E

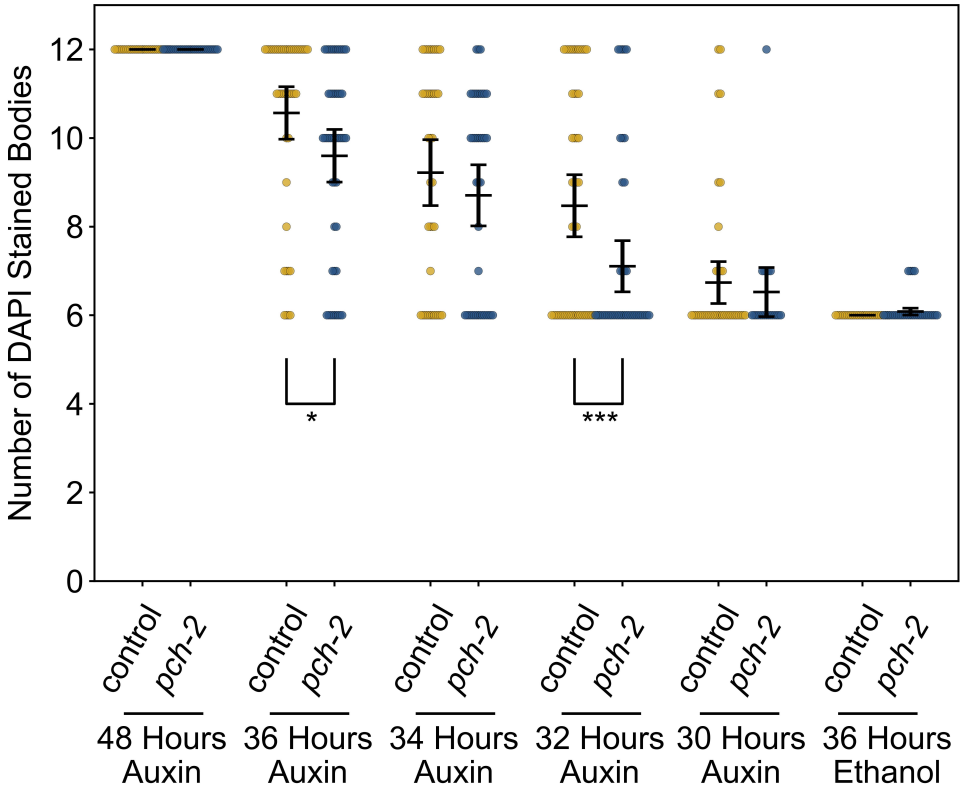

Figure 4

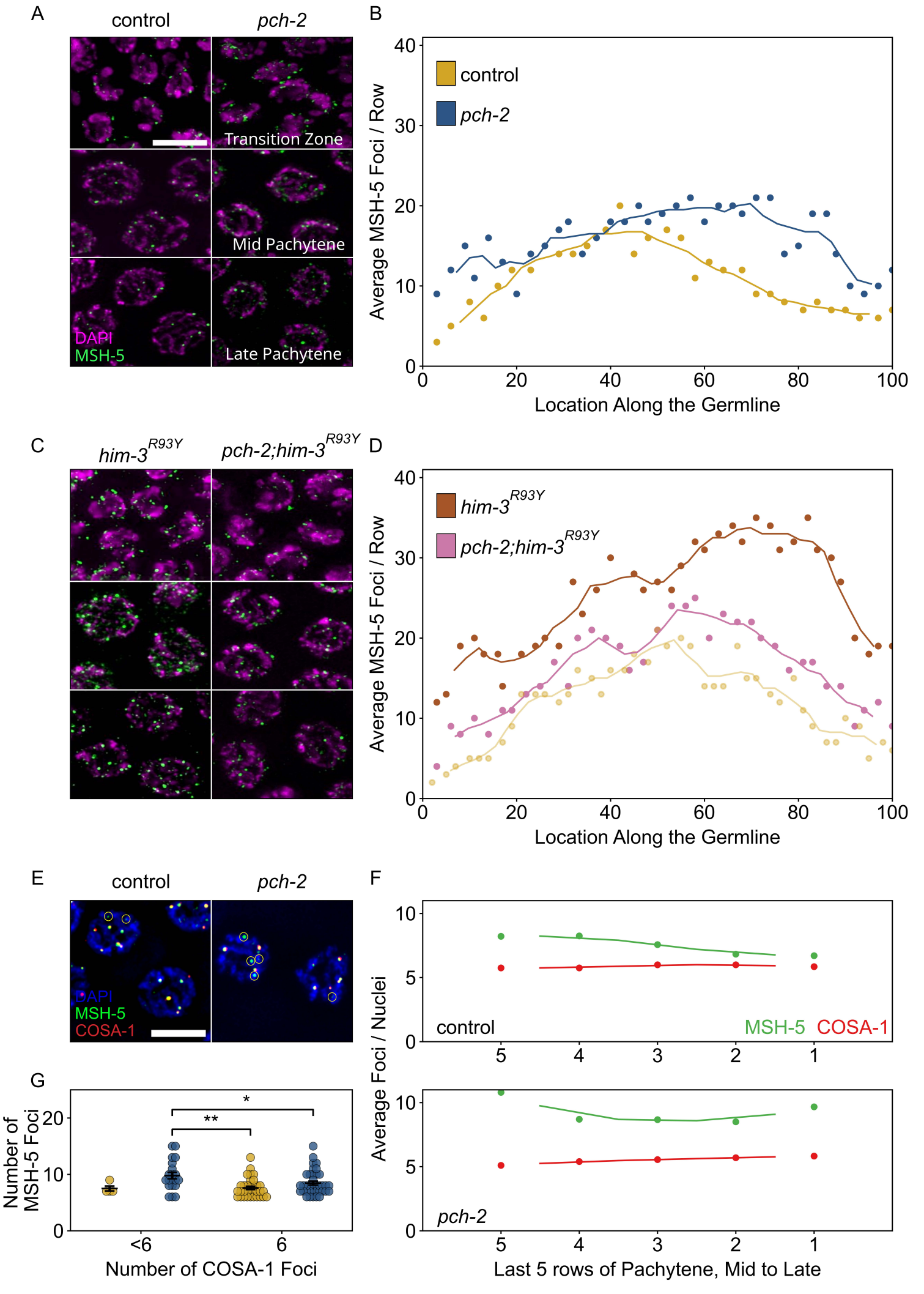
A
control
pch-2
Transition Zone
Mid Pachytene
Late Pachytene
DAPI
MSH-5
B
control
pch-2
Average MSH-5 Foci / Row
Location Along the Germline
C
him-3R93Y
pch-2;him-3R93Y
D
him-3R93Y
pch-2;him-3R93Y
Average MSH-5 Foci / Row
Location Along the Germline
E
control
pch-2
DAPI
MSH-5
COSA-1
F
control
MSH-5
COSA-1
pch-2
Average Foci / Nuclei
Last 5 rows of Pachytene, Mid to Late
G
Number of MSH-5 Foci
Number of COSA-1 Foci
<6
6
*
**

A

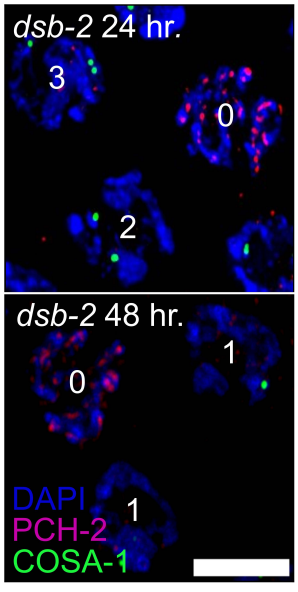
dsb-2 24 hr.
3
0
2
dsb-2 48 hr.
1
0
1
DAPI
PCH-2
COSA-1

B

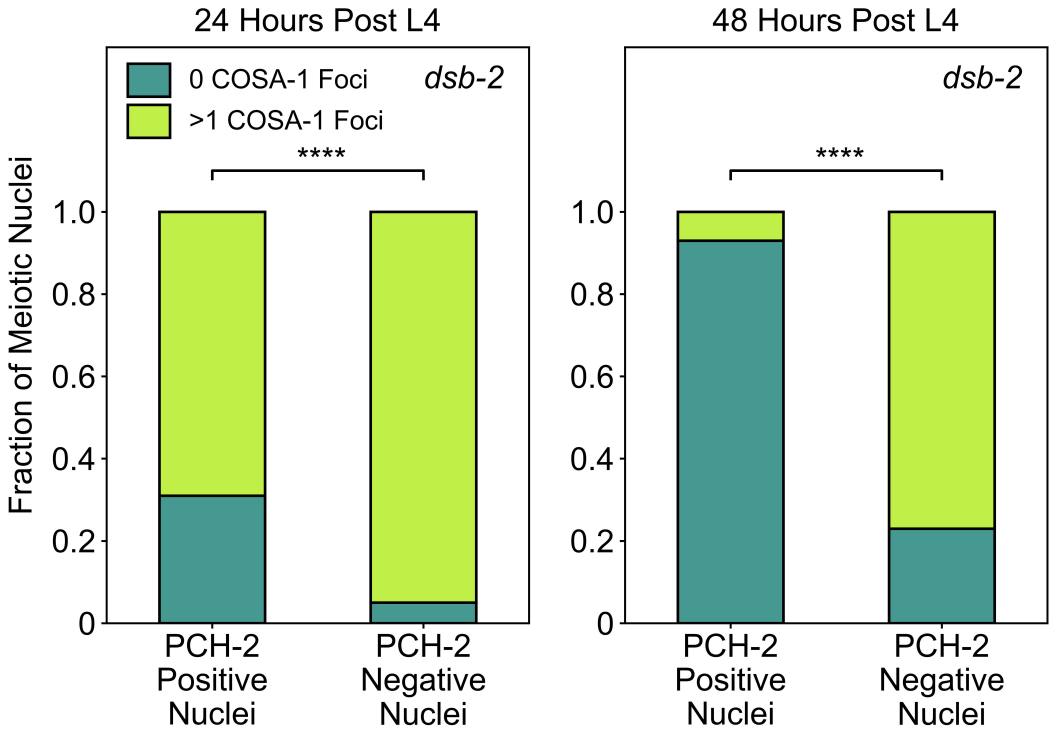
24 Hours Post L4
48 Hours Post L4
0 COSA-1 Foci
>1 COSA-1 Foci
dsb-2
****
Fraction of Meiotic Nuclei
1.0
0.8
0.6
0.4
0.2
0
PCH-2 Positive Nuclei
PCH-2 Negative Nuclei

C

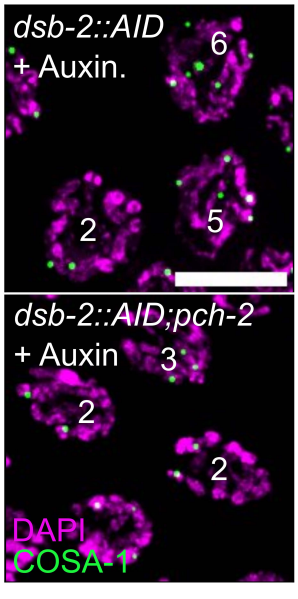
dsb-2::AID
+ Auxin.
6
2
5
dsb-2::AID;pch-2
+ Auxin
3
2
2
DAPI
COSA-1

D

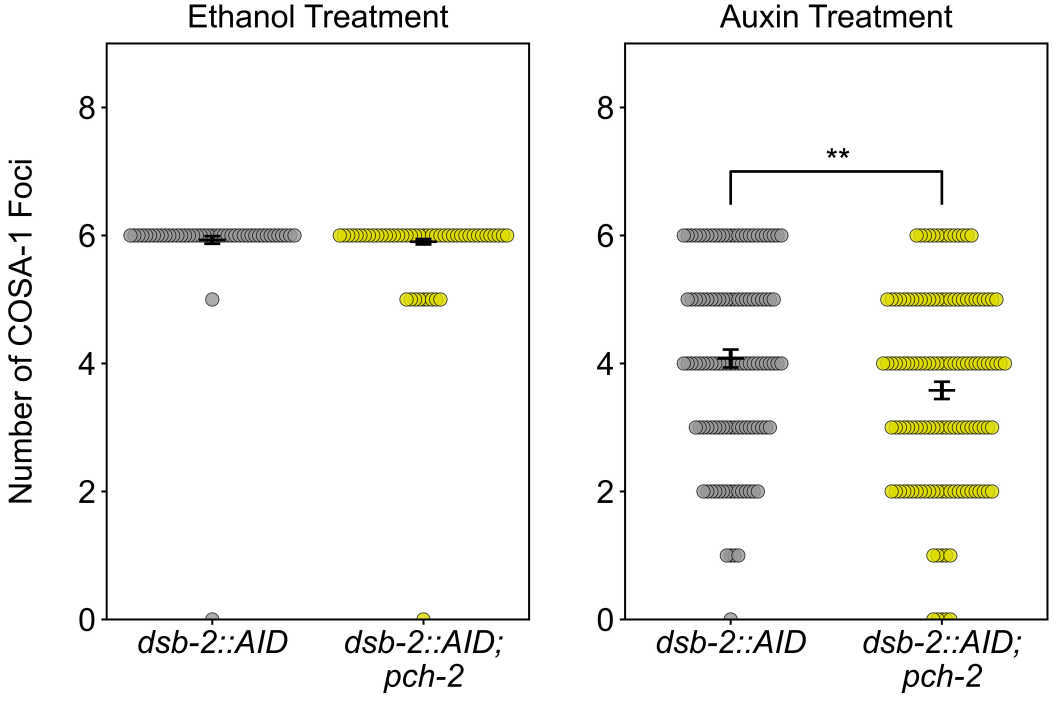
Ethanol Treatment
Auxin Treatment
Number of COSA-1 Foci
8
6
4
2
0
**
dsb-2::AID
dsb-2::AID; pch-2

Figure 6

A

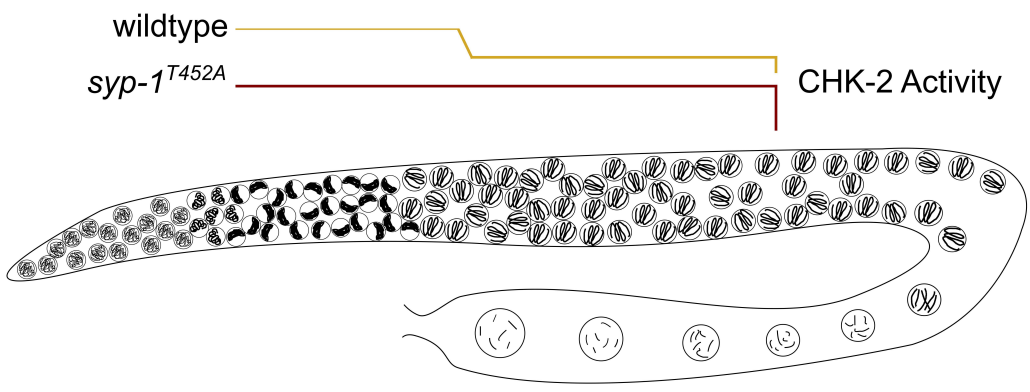

B

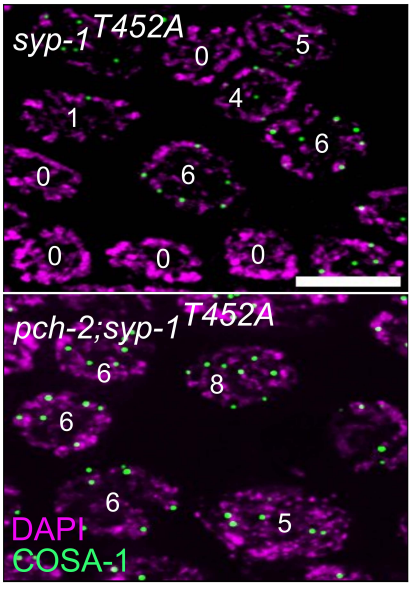

C

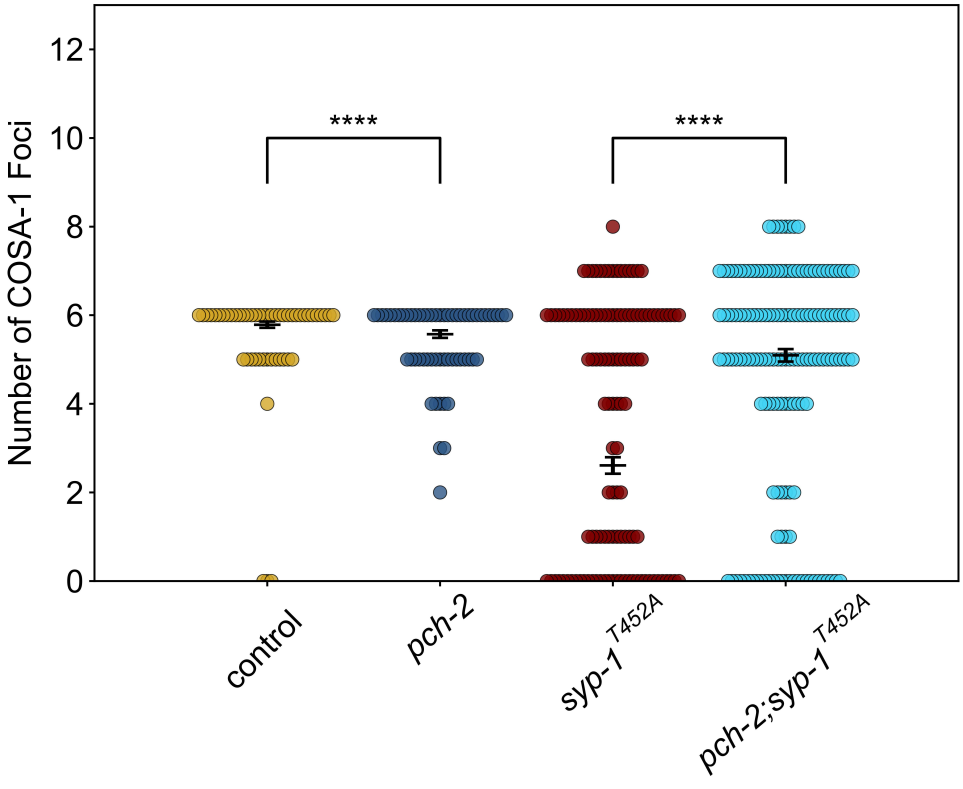

D

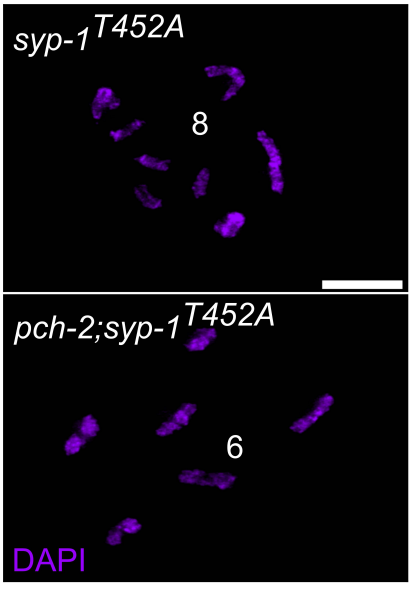

E

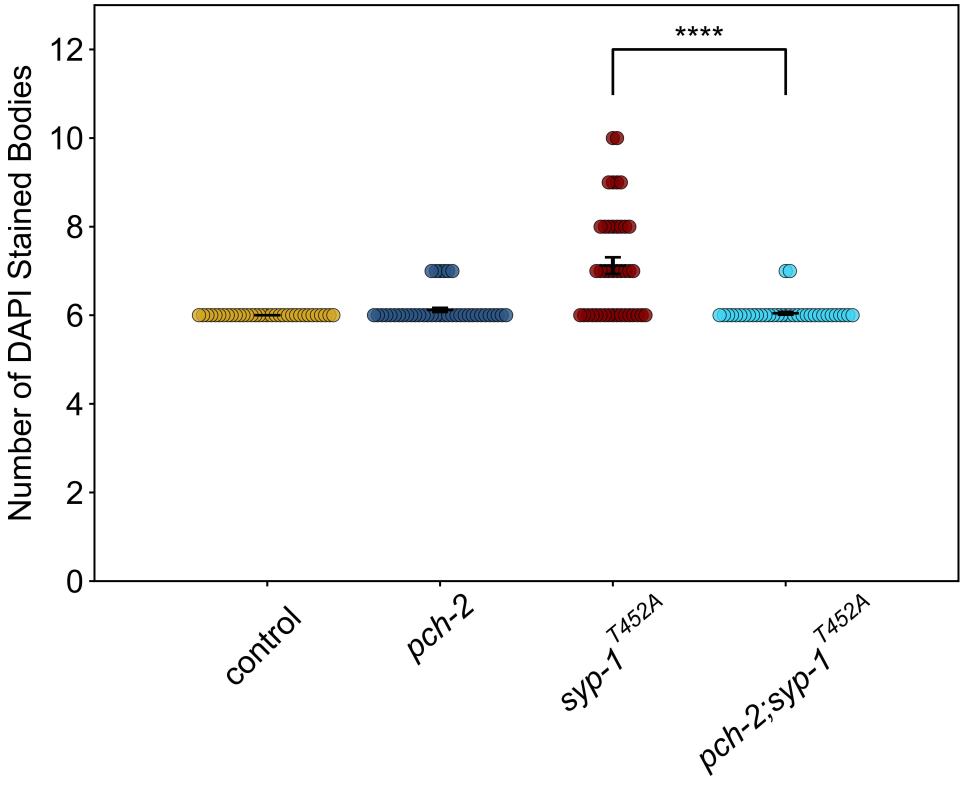

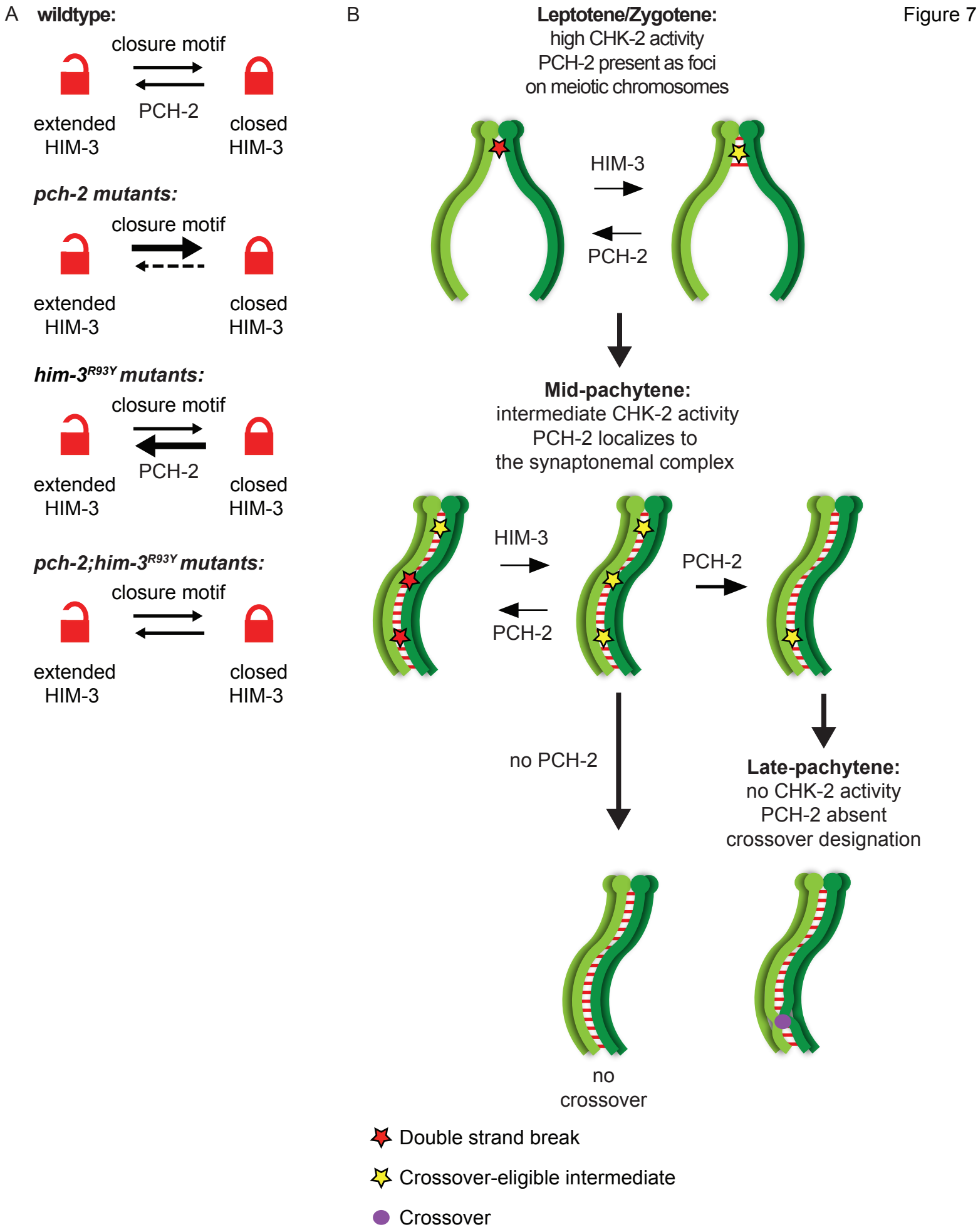
A
wildtype:
closure motif
PCH-2
extended HIM-3
closed HIM-3
pch-2 mutants:
closure motif
extended HIM-3
closed HIM-3
him-3R93Y mutants:
closure motif
PCH-2
extended HIM-3
closed HIM-3
pch-2;him-3R93Y mutants:
closure motif
extended HIM-3
closed HIM-3
B
Leptotene/Zygotene:
high CHK-2 activity
PCH-2 present as foci
on meiotic chromosomes
HIM-3
PCH-2
Mid-pachytene:
intermediate CHK-2 activity
PCH-2 localizes to
the synaptonemal complex
HIM-3
PCH-2
PCH-2
no PCH-2
Late-pachytene:
no CHK-2 activity
PCH-2 absent
crossover designation
no
crossover
Double strand break
Crossover-eligible intermediate
Crossover

Figure 7

Supplementary Table 1: Single nucleotide polymorphisms used for recombination assay

Chromosome and SNP	Primer Name	Primer Genetic Location	Primer Sequence FOR	Primer Sequence REV	Restriction enzyme	N2	HI
IA	F56C11	-19	ATGCCAGTGATAAGGAACGG	TCACATCCCTTGTCGATGAA	DraI	354, 146	500
IB	Y71G12	–12.3	GACAATGACCAATAAGACG	GATCCGTGAAATTGTTCCG	BsrI	440, 125	364, 125, 76
IC	K04F10	0.9	ATCATTCTCCAGGCCACGTTAC	CTGAACTAGTCGAACAAACCCC	NdeI	594	300, 294
ID	T07D10	13.6	CTTGGTGTGGGGAGAGTATAGG	TTTGTCCGGATTGACTCTGC	Sau3AI	303, 63	207, 96, 63
IE	ZK909	28.8	CACAAGTGGTTTGGAAGTACCG	CAACAAAGGGATAGATCACGGG	HindIII	450	236, 214
IIIA	pkP3081	-26.98	AGCAAGAATGAGCCGATTG	GTCGGCCGTTTTCAAATAACTG	TaqI	222, 149	195, 145, 27
IIIB	pkP3095	-5.12	TCTCGTCAATTGTCGCCTG	TTATTTGCAATCCAACGGC	ApoI	308	168, 140
IIIC	pkP3101	-0.9	CCAAGTGCAAACTATGGTGC	ATAAACAATTTCAGTGCCGC	HinfI	495	282, 213
IIID	pkP3035	0.9	CGTAAACTACCAAACTCGGTG	GGTCTACTACAACTATACAGGC	Eco0109I	732	419, 313
IIIE	pkP3080	21.29	CGGTGGTGGTAAAAGTGTAAC	CAACATTCAGGCTGTGCTTTCC	Hpy188III	365, 76, 68, 35	241, 124, 76, 68, 35
IVA	F56B3	-24	TGATGGTGTGTCTGCGTACC	AGAGCTGGAGAGCACGGATA	DraI	301, 128, 71	429, 71
IVB	F52C12	−14.9	ACATTTAGTCACGCGTAGGG	GCCCGAATCTAGCACATAAG	HpaII	191, 137, 22	328, 22
IVC	B0273	1.8	AATACAGCAGTCGTTCCGTTC	TGAACTTCATGAACCAGCTTG	DraI	288, 144	432

IVD	K10D11	6.7	GATTATTTCAGAGGAGCAGAGC	CATAGCACGTGGAATAACCAC	HindIII	420	245, 175
IVE	T02D1	16.8	TGCTTAAAGTCATCGTGTCCAC	TGTAAACCGTATCGAATCCGAC	EarI	174, 235	408
XA	pkP6139	-19.97	AAGAGTGAACCTTTTCCGTGAG	TGATGCAATTTATACACACGCC	MseI	401, 31	279, 122, 31
XB	pkP6120	-10.46	TCGTGGCACCATAAAAGTG	GATTCAGATCAAACAGAGGTGG	DraI	243	128, 115
XC	pkP6157	-0.14	GGGGTATAATGAACCAACCTG	TGTAGGAACCGTTTGTTTCTTC	ApoI	261, 48	150, 111, 48
XD	pkP6161	9.38	ATCGACCCCAACAATGCAC	TCCGTCATCCAAATCTCCG	AseI	542	287, 255
XE	pkP6170	24.07	CGCTGTCACAATCTCTAAAATG	AAACCCTCCCCACTTTGTTGTC	ApoI	249, 118, 56	197, 118, 56, 52

Supplementary Figure 1

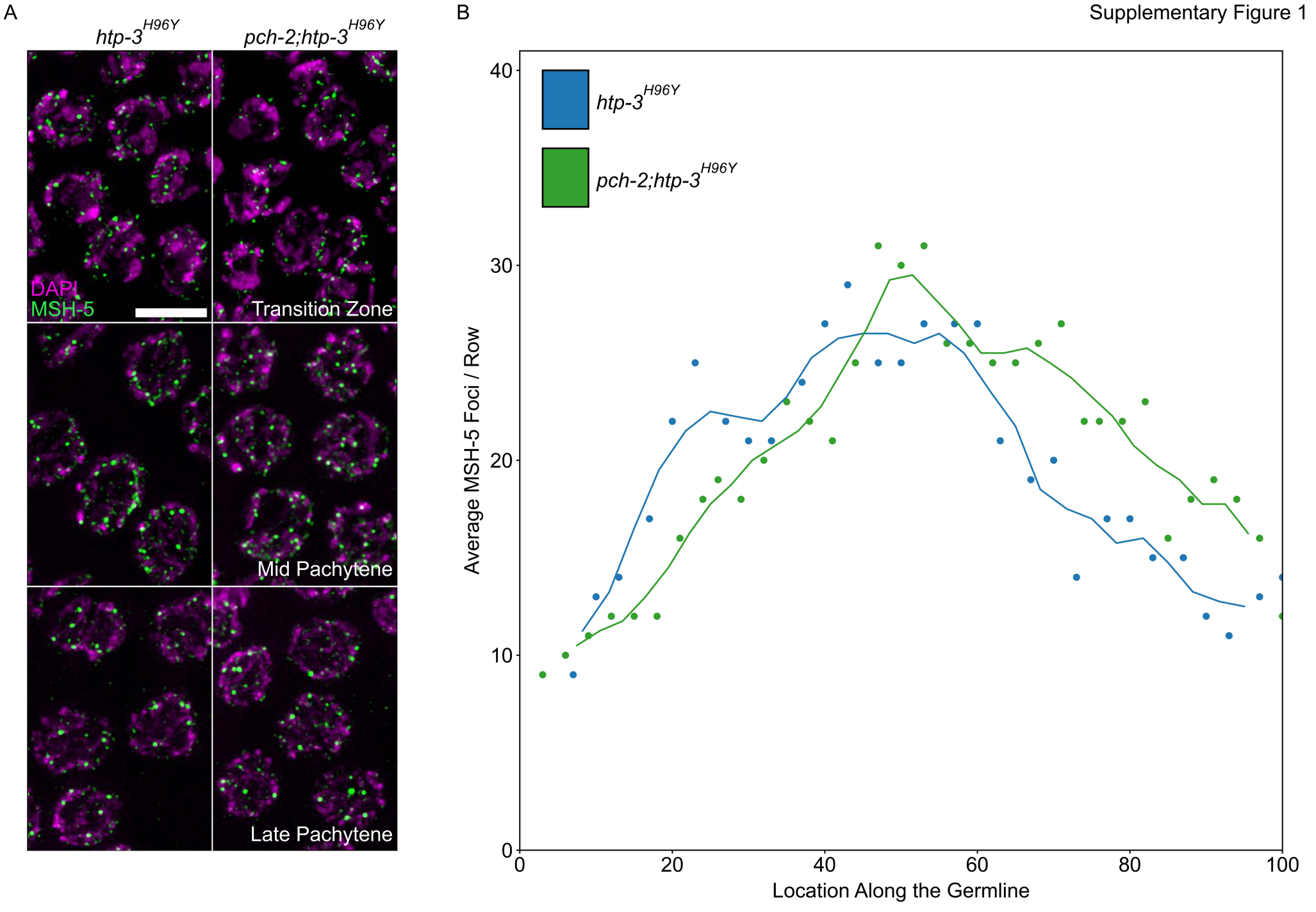
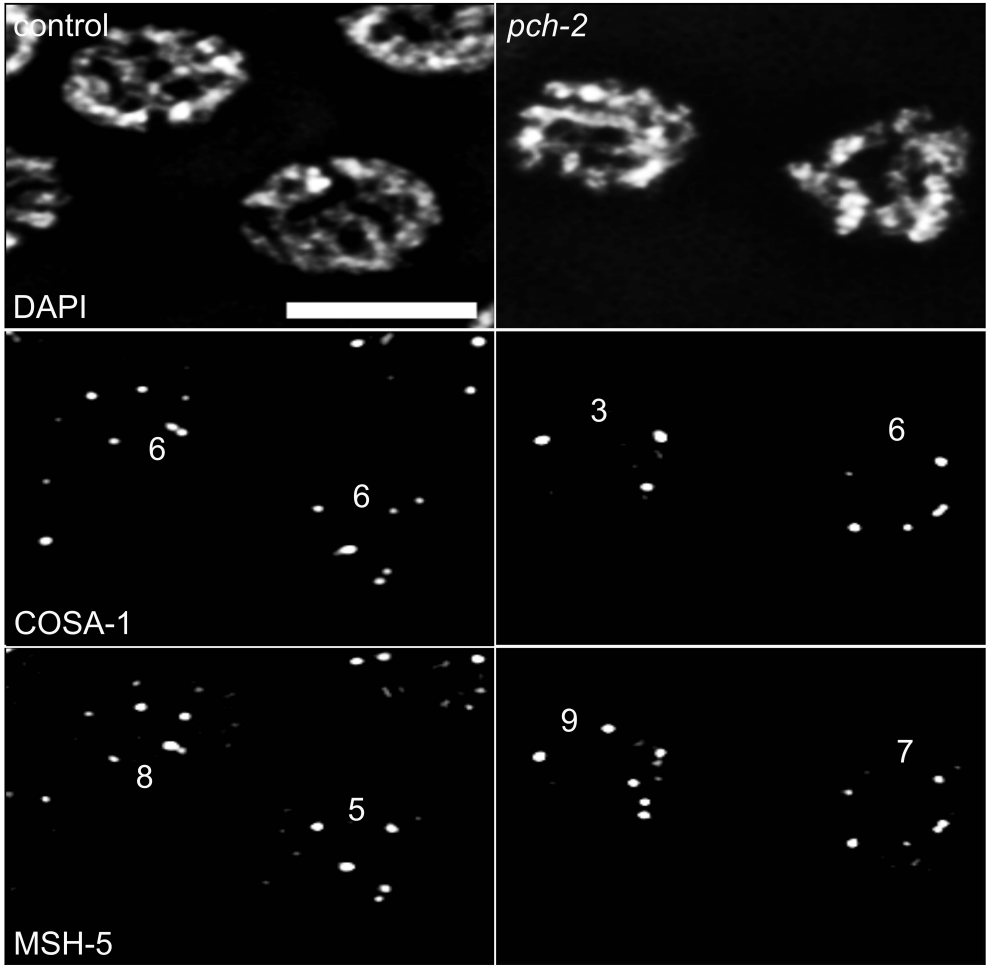
A